

© Copyright 2017

Chuchuan Hong

# Meta-form near eye visor

Chuchuan Hong

A thesis

submitted in partial fulfillment of the  
requirements for the degree of

Master of Science in Electrical Engineering

University of Washington

2017

Committee:

Arka Majumdar

Lih-Yuan Lin

Program Authorized to Offer Degree:

Electrical Engineering

University of Washington

**Abstract**

Meta-form near eye visor

Chuchuan Hong

Chair of the Supervisory Committee:  
Dr. Arka Majumdar  
Electrical Engineering

This thesis is about meta-form near-eye visor (NEV). Near eye visor is the core component in a head mounted display (HMD), because it directly decides the quality and volume of HMD.

Regarding freeform NEV, a limitation on Field of View (FOV) is proposed. A flat shape phase mask visor, termed here as meta-form visor, is used to replace the freeform NEV to lift the limitation. Metasurface is chosen to work as the visor, because of its flat surface and capability to implement spatial modulation to incident light wave. Metasurface is a two-dimensional array of subwavelength scatterers. Meta-form visor's vision performance is simulated in Zemax. Image simulation using the designed metasurface is performed in Lumerical FDTD. In this design dielectric material is chosen to compose the metasurface, for its lower loss in visible frequency than metallic metasurface.

# TABLE OF CONTENTS

List of Figures .....	iii
Chapter 1. Introduction and Review .....	1
1.1 Near Eye Visor.....	1
1.2 Metasurfaces and Metamaterials.....	2
1.3 Thesis Plan and Overview .....	3
Chapter 2. Fundamentals and Background .....	6
2.1 Electromagnetism .....	6
2.1.1 Maxwell’s Equations and Wave Funtion.....	6
2.1.2 Reflection and Refraction at Dielectric Interface .....	8
2.1.3 Dielectric subwavelength Scatterers .....	11
2.1.4 Metasurface Scatterers .....	13
2.2 Geometric Phase .....	14
2.2.1 Jones Calculus.....	14
2.2.2 Pancharatnam-Berry Phase .....	15
2.2.3 Fermat’s Principle and Generalized Snell’s Law.....	18
2.3 Evaluators to NEV .....	20
2.3.1 Modulation Transfer Function .....	20
2.3.2 Geomtric Opitcs .....	23
2.3.3 Field of View .....	25
Chapter 3. Results and Simulations .....	27

3.1	Freeform NEV .....	27
3.1.1	Freeform Visor Design and Limitation.....	27
3.1.2	Freeform Visor Performance .....	31
3.2	Meta-form NEV .....	33
3.2.1	Meta-form Visor Design.....	33
3.2.2	Phase Distribution on Meta-form Visor.....	35
3.2.3	Meta-form Visor Performance.....	37
3.3	Metasurface Design .....	41
3.4	Metasurface NEV image simulation.....	43
Chapter 4. Summary and Future work.....		47
4.1	Summary.....	47
4.2	Outlook and Future Work.....	48
Bibliography .....		50

## LIST OF FIGURES

Figure 1: Examples of products of head mounted display/ near eye visor from Sony, Microsoft and Google[1-3]. .....	2
Figure 2: Properties of TE wave and TM wave when light wave meets interface. Cross means arrow pointing inside plane away from reader, while dot means arrow pointing outside plane towards readers. ....	9
Figure 3: Reflectance and transmittance. ....	10
Figure 4: Model for Lewin’s theory. ....	12
Figure 5: Model of Poincare Sphere used to indicate phase difference of two points on it. ....	16
Figure 6: Light reflection on interface with phase shift. ....	19
Figure 7: Schematic to Anomalous reflection. ....	20
Figure 8: Definition of spatial frequency. ....	21
Figure 9: Appearance of two types of common distortion. ....	23
Figure 10: Explanation of how Field Curvature happens. ....	24
Figure 11: Explanation of how Coma happens. ....	25
Figure 12: The definition of field of view. ....	25
Figure 13: Side view of the schematic of the methodology of designing a near visor. ....	27
Figure 14: Formation of freeform NEV. ....	27
Figure 15: The schematic of freeform NEV. ....	28
Figure 16: Matlab result of (a)3D and (b) side view of freeform NEV system. ....	28
Figure 17: Physically invalid solution for freeform NEV as large FOV given. ....	29
Figure 18: Results from curve fitting, black surface being original and colored surface being fitted. ....	30
Figure 19: Vision performance of freeform NEV. ....	31

Figure 20: Schematics of meta-form visor on XZ plane. ....	32
Figure 21: 3D schematic of meta-form NEV. ....	33
Figure 22: Methodology of phase calculation. ....	34
Figure 23: Phase profile. ....	35
Figure 24: MTF of NEV. ....	36
Figure 25: Gird Distortion of NEV. ....	37
Figure 26: Ray tracing of NEV. ....	37
Figure 27: Liou & Brennan 1997 eye model. ....	38
Figure 28 Image simulation of Mona-Lisa. ....	38
Figure 29: 2-dimensional array structure of a metasurface and one pixel of this type of metasurface. .....	39
Figure 30: RCWA results, filling factor of one period to phase/ Amplitude response of reflection light. ....	40
Figure 31: Diameter map of scaled-down metasurface. ....	41
Figure 32: Real appearance of metasurface in Lumerical. ....	41
Figure 33: Schematic of display simulation and its result. ....	42
Figure 34: Schematic of the scale-down NEV system and energy distribution from sideview. ....	42
Figure 35: Results of image simulation. ....	44
Figure 36: RCWA result of Silicon Nitride post. ....	46
Figure 37: Phase mask after phase wrapping. ....	47

## **ACKNOWLEDGEMENTS**

Here, I sincerely acknowledge my advisor Professor Arka Majumdar for his patience and advising to this thesis project. His impressive amount of knowledge deeply stimulates me to work hard on my thesis. I also acknowledge Professor Lih-Yuan Lin to be my thesis defense committee. Her questions guide the direction to improve results from this thesis. I would like to appreciate kindness and help from every member from our laboratory, as well. Especially for Alan and Shane I really appreciate their help in designing the metasurface and their permission for citing their research results. Finally, I want to acknowledge my family for their support during these two years.

# CHAPTER 1: INTRODUCTION AND REVIEW

## 1.1 NEAR EYE VISOR

Augmented reality (AR) and virtual reality (VR) technologies are popular in recent years. Head mounted display (HMD) is one of the most suitable platform for AR/VR technology. Near-eye visor (NEV) generated great interest among researchers in academia and industries, for its potential to be used in head-mounted display (HMD). There have been products from big companies such as Sony[4], Google[5], Microsoft[6], Nokia[7] and etc. Examples of HMD products from Sony, Microsoft and Google[1-3] are shown in Figure.1. Briefly, NEV is a vision system that couples lights from display into human's eye. Most of the existing NEVs operate based on the principle of ray optics, i.e., Snell's Law. Specifically, when the visor comes close to the eye, light needs to be bent at steeper angles to maintain the desired FOV, and often the range is restricted. Various methods, including, freeform optics [8-11], optical waveguides [12], reflective system [13, 14] or retinal scanning technology [15] are reported to reach large field of view or large exit pupil distance. For example, Y. Zhu et al. [13] designed an eight-mirror reversed telescoped reflective system to accomplish an ultra-thin near-eye device; D. Cheng et al. [16] combined geometrical waveguides technology with freeform optics technology for a design of ultra-thin near-eye display; J. Yang et al. designed a see-through near-eye display using geometrical waveguides to accomplish a large FOV [12]; O. Cakmakci et al. [8] proposed a freeform single-element head-worn display: they used a 289 terms Gaussian radial basis function for representing freeform optical surface as a magnifier and reflector. However, in all these designs, FOV is limited. In the single-element head-worn display design, the full

diagonal FOV is around  $24^\circ$  [8]. The design from J. Yang et al. [12] with large FOV is reported to have horizontal FOV of  $30^\circ$  and vertical FOV of  $60^\circ$ .



Figure 1: Examples of products of head mounted display/ near eye visor from Sony, Microsoft and Google[1-3].

## 1.2 METASURFACES AND METAMATERIALS

To efficiently control light wave in manners which are not achievable in nature, artificial structures/ materials are investigated intensely during the past 15 years. Among them, metamaterial is one of the most popular topics.

Metamaterials, where ‘meta’ means ‘beyond’ from Greek, is an artificial structure made of subwavelength periodic ‘meta-atom’ [17]. Theoretically, metamaterials can give electric response and magnetic response not available in nature [18]. Such discovery leads us into a new physics world with negative refractive index [19], superresolution imaging [20] or invisible cloaking [21]. However, challenges still exist in today’s metamaterial research. For example, loss and high dispersion under visible frequency in metallic metamaterials restrict their applications in visual optics regime [18]. Besides, fabrication of a bulky 3D structure with ultra-meticulous spatial arrangement is still challenging.

In contrast, 2D planer metamaterials, called metasurfaces, attract high attention. An optical metasurface is two-dimensional array of sub-wavelength scale scatters which can arbitrarily modify the incident optical wavefronts with sub-wavelength resolution. Due to their compact structure and scale, metasurfaces can be fabricated using the standard semiconductor nanofabrication technology. The

metasurfaces are similar to the conventional diffractive optics, but due to its sub-wavelength nature, the metasurfaces can provide multiple phase-shifts changing the lateral geometry. Hence, the metasurface can be fabricated using a single lithography stage, whereas for conventional diffractive optics multi-stage lithography is generally needed. Metasurfaces enable flat, and extremely thin ( $\sim 1\mu\text{m}$ ) optical elements and thus they can be easily integrated into optical systems with low spatial and weight consuming. Recently, our group has demonstrated metasurfaces in visible frequencies using silicon nitride, and also reported operating of freeform optical elements using metasurfaces [22].

In 2011, reflection/refraction on interface with abrupt phase shift was reported by Yu, Capasso and et al[23]. From their research, we see anomalous reflection/refraction behaviors when phase gradient exists on interface. Although they used V-shaped metallic antennas[23] to compose a phase array, dielectric metasurface is able to work as a phase array, as well.

In visible regime, metallic materials are lossy due to their negative permittivity so that imaginary refractive index. Hence, recently, optical metasurfaces made of low-loss dielectric materials have caught high attention[18]. Low-contrast metasurface has been studied and fabricated by our group[22]. Using Silicon Nitride as the bricks to compose subwavelength scatterers, this metasurface has low loss in visible frequency and can be applied to make a lens or vortex beam generator[22]. For the same reason, to apply metasurfaces into human-vision system, dielectric metasurface is a better choice than metallic one.

### 1.3 THESIS PLAN AND OVERVIEW

Researches on either near eye visor or metasurface are young and rapidly growing. NEV or HMD is the optimal platform for AR/VR technology. Although results on high-quality NEV have been reported[8-10, 12-16], most of them have complex structures and limited FOV. Metasurface, as a flat surface, enables an ultra-compact structure of NEV to decrease volume and weight of HMD. Besides, dielectric metasurface is extremely attractive due to its low loss in visible regime, compared to metallic metasurface.

In this thesis, a combination of metasurface with NEV device bridges the boundary from ray optics to electromagnetism. A design based on metasurface freeform optics is proposed. The term here is meta-form optics [24],

Chapter 2 briefly introduces physics fundamentals behind metasurfaces and near eye visor. Starting from Maxwell's equations, scattering of dielectric materials with comparable size to wavelength is shortly introduced. Results from this scattering indicate mechanism of how subwavelength scatterers work. Subwavelength scatterers are the building blocks of metasurface. By reasonably tailoring size of the those scatterers, they can generate instinct phase response. Thus, arrays of different subwavelength scatterers can be used to form a phase mask. Reflection on dielectric interface is engineered by the phase gradient on the interface, where we introduce the keystone in design of meta-form visor, the Generalized Snell's Law[23]. It can be interpreted by Fermat's principle and detailed proof is provided, as well. Besides, evaluators are described to assess the quality of NEV.

Chapter 3 depicts the design and simulation of NEV, step by step and in detail. Initiated from freeform NEV, I propose my own methodology to design a freeform NEV. Its performance is simulated in Zemax. By comparing our freeform visor with a published paper by other group, we verify the design methodology. Importantly, the limitation on FOV in freeform NEV is proposed here, which is due to the high curvature shape of the freeform visor. This limitation reflects the significance of meta-form NEV. Design of meta-form NEV is governed by Generalized Snell's Law and anomalous reflection. Based on Generalized Snell's Law, phase mask on meta-form visor is calculated. This phase mask is used in ray optics simulation in Zemax. Simulation results indicates that the meta-form NEV is capable to be used in a vision system. In detail, the modulation transfer function (MTF) of the visor is over 50% at 50 cycles/mm, which is enough for vision system[12]. The grid distortion is less than 9%. More importantly, it provides promising FOV values (both horizontally and vertically as  $77^\circ$ ) with closer distance from visor to eye (visor being 2.5cm

away from the eyes). Finally, a metasurface is introduced to realize this phase mask. And in Lumerical FDTD, an image simulation is carried on using the metasurface.

Chapter 4 concisely summarizes this thesis and points out future works for meta-form NEV. For example, in this thesis I use Silicon to compose the subwavelength scatterers, and this NEV is suitable for VR technology. If Silicon Nitride is used, but not Silicon, this NEV will be suitable for AR application. Besides, the meta-form NEV should be improved to work under RGB frequencies in practice.

## CHAPTER 2: FUNDAMENTALS AND KNOWLEDGE

### BACKGROUND

#### 2.1 ELECTROMAGNETISM

##### 2.1.1 Maxwell's Equations and Wave Equation

Maxwell's Equations depict the behaviors of light/ electromagnetic field in medium, as shown below:

$$\nabla \times E = -\frac{\partial B}{\partial t} \quad (1)$$

$$\nabla \times H = J + \frac{\partial D}{\partial t} \quad (2)$$

$$\nabla \cdot D = \rho \quad (3)$$

$$\nabla \cdot B = 0 \quad (4)$$

where  $J$  is current density and  $\rho$  stands for charge density. Equation (1) ~ (4) describe Gauss's flux theorem, Gauss's Law for magnetism, Faraday's law of induction and Ampère's circuital law with Maxwell's corrections, respectively. In addition, relationship between electric field  $E$  and electric displacement  $D$ , or magnetic field  $H$  and magnetic flux density  $B$  are expressed in constitutive equations:

$$D = \epsilon E \quad (5)$$

$$B = \mu H \quad (6)$$

where  $\epsilon$  and  $\mu$  are electric permittivity and magnetic permeability, respectively. Specifically, permittivity and permeability are defined in the form of a constant derived from vacuum multiplied by a number determined by medium:

$$\epsilon = \epsilon_r \epsilon_0 \quad (7)$$

$$\mu = \mu_r \mu_0 \quad (8)$$

where  $\epsilon_0 = 8.85 \times 10^{-12} F/m$  is the permittivity in vacuum and  $\mu_0 = 4\pi \times 10^{-7} H/m$  is the permeability in vacuum.  $\epsilon_r$  and  $\mu_r$  are named as relative permittivity and permeability, respectively. Naturally, in non-magnetic media, value of relative permeability is 1.

Wave function is derived from Maxwell's equation mathematically. Based on the truth:  $\nabla \times (\nabla \times V) = \nabla(\nabla \cdot V) - \nabla^2 V$ , we firstly apply Nabla Operator on equation (1). Under condition of no existence of free charges or any currents, we shuffle order of time deviation and spatial deviation to obtain:

$$\nabla \times (\nabla \times E) = \nabla(\nabla \cdot E) - \nabla^2 E = \nabla \times \left( -\frac{\partial B}{\partial t} \right) = -\frac{\partial(\nabla \times B)}{\partial t} \quad (9)$$

It is now convenient to substitute equation (7) into (9) to have:

$$\nabla \times (\nabla \times E) = -\mu_0 \frac{\partial(\nabla \times H)}{\partial t} \quad (10)$$

Next, we transform this equation by plugging in equation (2), with the absence of currents:

$$\nabla \times (\nabla \times E) = -\mu_0 \frac{\partial(\nabla \times H)}{\partial t} = -\mu_0 \epsilon_r \epsilon_0 \frac{\partial^2 E}{\partial t^2} \quad (11)$$

Here we believe

$$\nabla \cdot E = 0 \quad (12)$$

because of the absence of free carriers  $\rho$ , and assuming the dielectric constant  $\epsilon_r$  does not change rapidly over the space.

By combining equations (9), (11) and (12), the light Wave Function is neatly written as:

$$\nabla^2 E = \frac{1}{v^2} \frac{\partial^2 E}{\partial t^2} \quad (13)$$

$v$  in Wave Equation represents the speed of light in medium. Here, we use the definition of speed of light being  $c = 3 \times 10^8 \text{ m/s}$  in vacuum. Refractive index in a non-magnetic material is  $n = \sqrt{\epsilon_r}$ . Hence, speed of light in medium is defined as:  $v = c/n$ .

The plane wave solution for light wave function is used significantly in later chapters.

### 2.1.2 Reflection and Refraction at Dielectric Interface

When a plane wave meets the interface of a dielectric medium, the plane wave can be decomposed into TE wave and TM wave, as shown in figure below.

Let us assume all the light waves are plane waves (i for incident light, r for reflected light and t for refraction light):

$$\vec{E}_i = \vec{E}_{0i} \exp[i(\vec{k}_i \cdot \vec{r} - \omega_i t)] \quad (14)$$

$$\vec{E}_r = \vec{E}_{0r} \exp[i(\vec{k}_r \cdot \vec{r} - \omega_r t)] \quad (15)$$

$$\vec{E}_t = \vec{E}_{0t} \exp[i(\vec{k}_t \cdot \vec{r} - \omega_t t)] \quad (16)$$

Based on boundary condition: both the transverse electric and transverse magnetic fields must be continuous:

$$(\vec{E}_i + \vec{E}_r) \times \vec{n} = \vec{E}_t \times \vec{n} \quad (17)$$

where  $\vec{n}$  is surface normal vector.

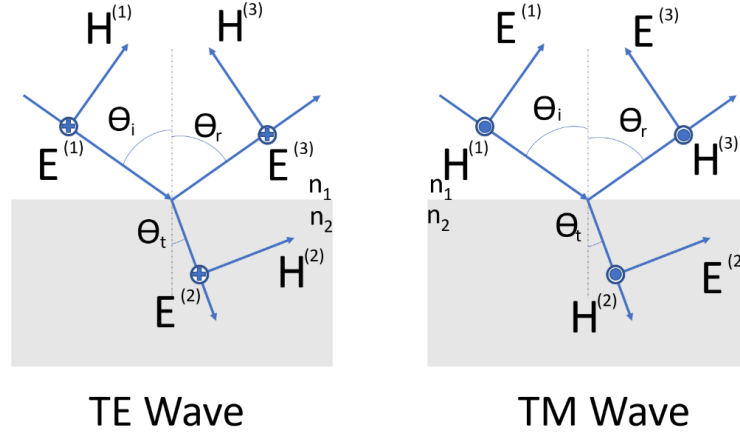


Figure 2: Properties of TE wave and TM wave when light wave meets interface. Cross means arrow pointing inside plane away from reader, while dot means arrow pointing outside plane towards readers.

For electric component of TE wave and magnetic component of TM wave, boundary condition is written as:

$$E_{i_{TE}} + E_{r_{TE}} = E_{t_{TE}} \quad (18)$$

$$H_{i_{TM}} - H_{r_{TM}} = H_{t_{TM}} \quad (19)$$

while in terms of magnetic component of TM wave and electric component of TE mode, boundary condition should hold, as well:

$$H_{i_{TE}} \cos \theta_i - H_{r_{TE}} \cos \theta_r = H_{t_{TE}} \cos \theta_t \quad (20)$$

$$E_{i_{TM}} \cos \theta_i + E_{r_{TM}} \cos \theta_r = E_{t_{TM}} \cos \theta_t \quad (21)$$

Under condition that  $\sqrt{\mu}H = \sqrt{\epsilon}E$ , we define relative refractive index  $n = n_2/n_1$ . Accordingly, reflection coefficients and refraction coefficients for TE or TM wave are obtained:

For TE wave:

$$r_{TE} = \frac{\cos \theta_i - n \cos \theta_t}{\cos \theta_i + n \cos \theta_t} \quad (22)$$

$$t_{TE} = \frac{2 \cos \theta_i}{\cos \theta_i + n \cos \theta_t} \quad (23)$$

For TM wave:

$$r_{TM} = \frac{-n \cos \theta_i + \cos \theta_t}{n \cos \theta_i + \cos \theta_t} \quad (24)$$

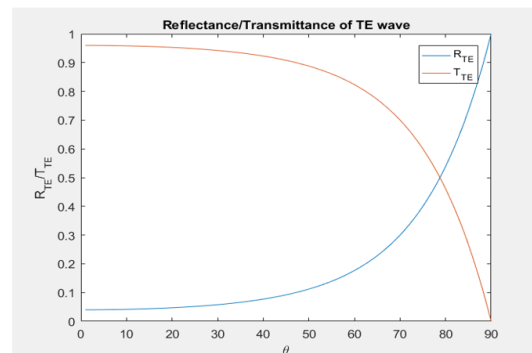
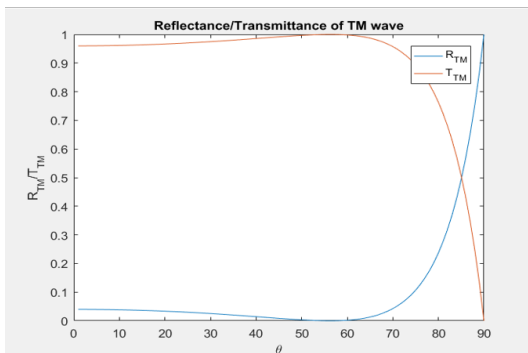
$$t_{TM} = \frac{2 \cos \theta_i}{n \cos \theta_i + \cos \theta_t} \quad (25)$$

Reflectance is defined as the ratio of reflection energy to incident energy and expressed in  $R = |r|^2$ .

Transmittance is defined as the difference from reflectance to 1:  $T = 1 - R$ .

In figure below, reflectance and transmittance in various conditions are shown, for both TE and TM waves:

Internal reflection/refraction ( $n_2 < n_1$ )



external reflection/refraction ( $n_2 > n_1$ )

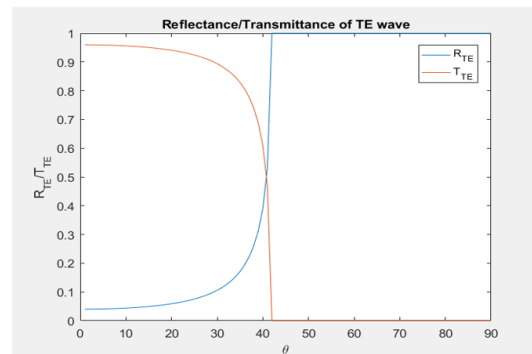
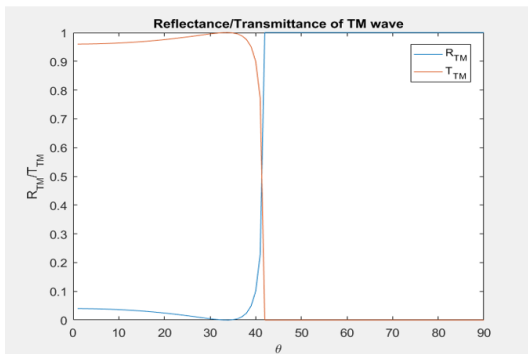


Figure 3: Reflectance and transmittance

In terms of phase response from reflection/refraction at dielectric interface, it varies from TE to TM waves and is related to the sign of reflection coefficients  $r$ .

For both TE and TM wave, refraction coefficient  $t$  is always positive, hence refraction light keeps the same phase as incident light. However, for reflection light, reflection coefficient  $r$  is not always positive. Besides positive, it will be negative or even imaginary. In non-positive reflection coefficient situation, phase response for TE and TM wave is valuable to be investigated.

In the modeling of metasurface, a three-layer system should always be considered, with air, metasurface and substrate. It is given by [25], without derivation here,

$$r = \frac{r_{12} + r_{23}e^{-2i\delta}}{1 + r_{12}r_{23}e^{-2i\delta}} \quad (26)$$

$$t = \frac{t_{12}t_{23}e^{-2i\delta}}{1 + r_{12}r_{23}e^{-2i\delta}} \quad (27)$$

Here  $\delta = \frac{2\pi d}{\lambda} n_2 \cos\theta_2$ ,  $d$  is the thickness of inner layer (metasurface) with refractive index of  $n_2$ .

$\theta_2$  is the refracted angle from outer layer to inner layer.

### 2.1.3 Dielectric Subwavelength Scatterers

So far, we have discussed media with uniform refractive index, regardless of direction or wavelength of the light interacting with them. However, most media are inhomogeneous or dispersive[26]. Hence in a metasurface, its subwavelength scatterers cannot be studied based on the simple theories in the former chapter.

Electric response or magnetic response from dielectric from dielectric metasurface can be tuned by tailoring geometry of scatterers on the metasurface. Besides, dielectric metasurface possesses less loss than metallic metasurface. Hence, in this thesis, I am focusing on dielectric metasurface.

In dielectric metamaterials, Mie resonances generate electric dipole and magnetic dipole like fields through displacement current[26, 27]. Mie scattering, also called Lorenz-Mie solution to Maxwell equations, is suitable to depict the scattering when wavelength of electromagnetic wave is comparable to size of scatterers.

Based on theory proposed by Lewin in 1946[28], a negative effective permittivity  $\varepsilon$  is predicted. He investigated the response of permittivity and permeability in a model of a series of dielectric spheres  $(\mu_1, \varepsilon_1)$  embedded in an outer space  $(\mu_2, \varepsilon_2)$ [27]. This model is shown in Figure 4. Specifically, to the view of scattering theory, scattering field from an isolated dielectric sphere can be decomposed into fields from series of electric dipole field and magnetic dipole field. The  $m^{\text{th}}$  term of electric field is written as[27]:

$$a_m = \frac{n\Psi_m(nx)\Psi'_m(x) - \Psi_m(x)\Psi'_m(nx)}{n\Psi_m(nx)\xi'_m(x) - \xi_m(x)\Psi'_m(nx)} \quad (28)$$

The  $m^{\text{th}}$  term of magnetic field is written in:

$$b_m = \frac{\Psi_m(nx)\Psi'_m(x) - n\Psi_m(x)\Psi'_m(nx)}{\Psi_m(nx)\xi'_m(x) - n\xi_m(x)\Psi'_m(nx)} \quad (29)$$

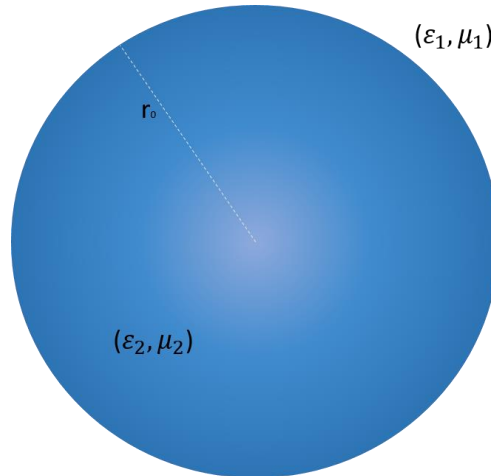


Figure 4: Model for Lewin's theory

where  $x = k_0 r_0$ .  $k_0$  is the free-space wavenumber and  $r_0$  is the radius of spherical scatterers.  $\Psi_m(x)$  and  $\xi_m(x)$  are Riccati-Bessel functions[27].  $n$  is the refractive index. Primes denote the differentiation with respect to argument.

Derived from equation (28) and (29), based on effective medium theory[29], effective permittivity and permeability are expressed in equations:

$$\varepsilon_{eff} = \varepsilon_1 \left( 1 + \frac{3v_f}{\frac{F(x) + 2b_e}{F(x) - b_e} - v_f} \right) \quad (30)$$

$$\mu_{eff} = \mu_1 \left( 1 + \frac{3v_f}{\frac{F(x) + 2b_m}{F(x) - b_m} - v_f} \right) \quad (31)$$

where

$$F(x) = \frac{2(\sin x - x \cos x)}{(x^2 - 1) \sin x + x \cos x}, \quad b_e = \varepsilon_1 / \varepsilon_2, \quad b_m = \mu_1 / \mu_2, \quad v_f = \frac{4}{3} \pi \left( \frac{r_0}{a} \right)^3$$

is the volume fraction of the spherical particles and  $x$  in  $F(x)$  stands for  $x = k_0 r_0 \sqrt{\varepsilon_2 \mu_2}$ .  $r_0$  is the radius of spherical scatterers and  $a$  is lattice constant.

From equation (30) and (31), effective permittivity and permeability become negative when

$$\frac{3v_f}{\frac{F(x) + 2b_e}{F(x) - b_e} - v_f} < -1 \quad \text{and} \quad \frac{3v_f}{\frac{F(x) + 2b_m}{F(x) - b_m} - v_f} < -1, \quad \text{respectively.}$$

#### 2.1.4 Metasurface Scatterers

Based on theory described in the former chapter, tuning size of dielectric scatterers can modulate electric response and magnetic response after scattering. Thus, light-matter interaction can be controlled. However, an easy and low-cost fabrication method for 3D optical metamaterials has not been discovered[26]. On the contrary, 2D planer optical metasurface is able to implement spatial modulation on incident light wave effectively and metasurface is much easier to be fabricated than metamaterials.

Conventionally, a device is needed to apply phase modulation on control over wave amplitude, such as wave plate or lens. In such elements, significant propagation path length is required to generate abundant phase accumulation[26]. However, metasurface is found to be able to break this gradual phase accumulation process, but implement an abrupt phase shift onto incident wave at interface.

A dielectric metasurface is composed of dielectric subwavelength scatterers and can be considered as a two-dimensional grating. In nano-photonics, similar subwavelength grating structure is able to generate phase shift, as well. Based on the effective medium theory, effective indices on direction along the pitch of grating and perpendicular to pitch of grating are different. Analogous to birefringent crystal, subwavelength grating can create phase lag. However, effective medium theory is only valid when period of grating is much less than wavelength, where we call it ‘deep subwavelength’ regime. In our metasurface design, size of scatterers are comparable to wavelength. Thus, effective medium theory cannot be directly applied. But, to understand phase evolution of light, concept of effective refractive index is still a useful tool[30].

We consider the phase accumulation as lights propagates through the grating layer. Here, the dominant propagation of light lies in out-of-plane components[30], which means we consider scatterers on metasurface as truncated waveguides. The waveguide can support low quality factor Fabry-Perot resonance, which is changing as size of scatterer is changing. Thus, phase response is changing consequently. Besides its capability to generate phase shifts, subwavelength scatterers confine energy only within 0<sup>th</sup> order diffraction, improving efficiency in intensity.

## 2.2 GEOMETRIC PHASE

### 2.2.1 Jones Calculus

Jones calculus is a powerful tool to describe the polarization light in any homogeneous isotropic non-attenuating medium[31]. Let us assume two transverse waves which are propagating along z-direction.

They can be expressed in the format of:

$$E_x = E_{0x} e^{i(kz - \omega t + \phi_x)} \quad (32)$$

$$E_y = E_{0y} e^{i(kz - \omega t + \phi_y)} \quad (33)$$

And the complex amplitude of the E field is written in terms of;

$$\begin{pmatrix} E_x(t) \\ E_y(t) \\ 0 \end{pmatrix} = \begin{pmatrix} E_x \\ E_y \\ 0 \end{pmatrix} = \begin{pmatrix} E_{0x} e^{i\phi_x} \\ E_{0y} e^{i\phi_y} \\ 0 \end{pmatrix} e^{i(kz - \omega t)} \quad (34)$$

By separating the propagator term of  $e^{i(kz - \omega t)}$  and leaving it aside, we call the remaining part in equation (34) as Jones Vector:

$$\begin{pmatrix} E_{0x} e^{i\phi_x} \\ E_{0y} e^{i\phi_y} \end{pmatrix} \quad (35)$$

Jones Vector is a concise representation to electromagnetic field of polarized light. It gives out the amplitude and phase of electric field in the x and y direction simultaneously. After dividing Jones Vector by  $E_0 = \sqrt{E_{0x}^2 + E_{0y}^2}$  for normalization, there are some useful examples of polarized light can be expressed in a neat form:

Linear polarized light along x-direction:  $\begin{pmatrix} 1 \\ 0 \end{pmatrix}$

Linear polarized light along y-direction:  $\begin{pmatrix} 0 \\ 1 \end{pmatrix}$

Right-handed circularly polarized light:  $\frac{1}{\sqrt{2}} \begin{pmatrix} 1 \\ +i \end{pmatrix}$

Left-handed circularly polarized light:  $\frac{1}{\sqrt{2}} \begin{pmatrix} 1 \\ -i \end{pmatrix}$

From Jones Vectors, phase information on x and y direction is clearly exhibited. When a Jones vector encounters an optical element, Jones Matrix is applied. In next chapter, Jones Matrix is used significantly to describe behavior of polarized light.

Like transfer matrix, the Jones Matrix of an arbitrary optical element is defined as a 2 by 2 matrix:

$$\begin{pmatrix} E_x^o \\ E_y^o \end{pmatrix} = \begin{pmatrix} T_{xx} & T_{xy} \\ T_{yx} & T_{yy} \end{pmatrix} \begin{pmatrix} E_x^i \\ E_y^i \end{pmatrix} \quad (36)$$

For example, if an optical device is able to create a Jones Matrix in form of  $\begin{pmatrix} e^{i\phi_x} & 0 \\ 0 & e^{i\phi_y} \end{pmatrix}$ , this device can generate an extra phase difference between x and y direction on Jones Vector. The underlying working principles of a wave plate (phase retarder) is based on such birefringence.

### 2.2.2 Pancharatnam-Berry phase

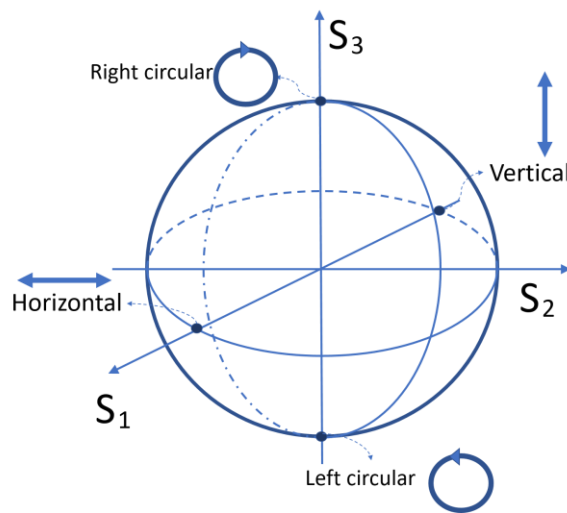


Figure 5: Model of Poincare Sphere used to indicate phase difference of two points on it.

Before discussing Pancharatnam-Berry phase, Poincare Sphere is introduced. Poincare Sphere is a useful tool for graphically describing polarization of light. Poincare Sphere was firstly proposed by French mathematician Henri Poincare [17] in the late 19<sup>th</sup> century. The model of Poincare Sphere is shown in figure below. It visualizes information carried by Jones vector or Stokes Vector. Stokes Vector contains polarization and intensity information in spherical coordinate. The three axes on Poincare Sphere correspond to the three parameters in Stokes Vector when intensity is neglected. Through tracing points on sphere surface and converting it from spherical coordinates into Cartesian Coordinate, Jones Vector can be

read out. The north pole and south pole on the sphere indicate two circular polarizations and equator represents linear polarization, while other positions represent elliptical polarization.

Now, Pancharatnam-Berry phase is discussed. Pancharatnam-Berry phase reveals the relationship between polarization state and phase of light[32]. Through Pancharatnam-Berry phase, we can understand mechanism of phase control to a more intuitive aspect. We can interpret Pancharatnam's discovery on Poincare Sphere. A closed path on the sphere is equivalent to a certain phase-shift. The phase-shift is equal to half of the area surrounded by the closed path [17].

As we know, subwavelength periodic structures can create phase change in terms of local change in polarization[33], rather than difference of wave path. In dielectric metasurface, subwavelength structures such as pillar[24, 34], rectangular [35] or oval [36], are introduced to form a 2D subwavelength grating providing phase shift. Based on theory regarding to Poincare Sphere and Jones matrix [31, 37], the most natural way to interpret Pancharatnam's discovery is derived as following.

Initially, we define effective permittivity tensor as:

$$\hat{\varepsilon} = \varepsilon_0 \begin{pmatrix} \varepsilon_1 & 0 \\ 0 & \varepsilon_2 \end{pmatrix} \quad (37)$$

Jones Matrix can be written in:

$$\hat{M} = \hat{R}(-\alpha) \begin{pmatrix} t_1 & 0 \\ 0 & t_2 \end{pmatrix} \hat{R}(\alpha) \quad (38)$$

when light is traveling through an anisotropic scatterer[18].  $t_1$  and  $t_2$  are coefficients of forward scattering along two optical axes.

$$\hat{R}(\alpha) = \begin{pmatrix} \cos \alpha & \sin \alpha \\ -\sin \alpha & \cos \alpha \end{pmatrix} \quad (39)$$

Equation (39) is the rotation matrix in cartesian coordinates.

The transmission matrix is written as:

$$\hat{M} = \begin{pmatrix} t_1 \cos^2 \alpha + t_2 \sin^2 \alpha & t_1 \cos \alpha \sin \alpha - t_2 \cos \alpha \sin \alpha \\ t_1 \cos \alpha \sin \alpha - t_2 \cos \alpha \sin \alpha & t_2 \cos^2 \alpha + t_1 \sin^2 \alpha \end{pmatrix} \quad (40)$$

In the basis of right-handed and left-handed circular polarization[38]:

$$\hat{M} = \begin{pmatrix} \frac{1}{2}(t_1 + t_2) & \frac{1}{2}(t_1 - t_2)e^{j2\alpha} \\ \frac{1}{2}(t_1 - t_2)e^{-j2\alpha} & \frac{1}{2}(t_1 + t_2) \end{pmatrix} \quad (41)$$

When a right-handed circularly polarized incident light is shone, the output light after the Jones Vector is written as:

$$E_T = \frac{t_1 + t_2}{2} \begin{pmatrix} 1 \\ 0 \end{pmatrix} + \frac{t_1 - t_2}{2} \exp(-j2\alpha) \begin{pmatrix} 0 \\ 1 \end{pmatrix} \quad (42)$$

So far, we found the possibility to modulate wavefront by spatially dependent phase shift term  $\exp(-j2\alpha)$ . Looking back onto Poincare Sphere, the angle  $\alpha$  here is a rotation angle of optical axis. Different from phase generated from light path difference, phase discontinuity here happens abruptly[38].

### 2.2.3 Fermat's Principle and Generalized Snell's Law

Phase response plays the vital role in metasurfaces. Behaviors of light reflected by interface with abrupt phase discontinuity is explained in this chapter.

Different from the nature of anomalous refraction generated by negative permittivity and negative permeability in bulk metamaterial or negative index materials, phase-discontinuous interface can be explained by Fermat's Principle.

Fermat's principle tells us that a ray of light goes through a space from one point to another along a stationary light path, which can give the least traveling time. The mathematical expression of Fermat's principle is written in:

$$\text{Optical Path Length (OPL)} = \int_A^B n(x, y, z) dl \quad (43)$$

where  $n$  is refractive index in the function of position. OPL is defined as the integral on products of refractive index multiplied by geometric path length of lights. To meet the requirement of ‘stationary light path’, we compare the actual light path to all possible light paths in its adjacent region, and equation (44) should be valid[39]:

$$\delta \text{OPL} = \delta \int_B^A n(x, y, z) dl = 0 \quad (44)$$

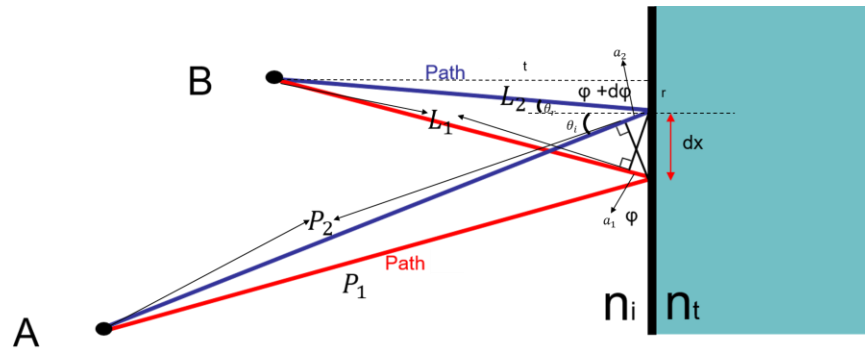


Figure 6: Light reflection on interface with phase shift

Using length marked in Figure 6, we can derive:

$$a_2 = dx \sin \theta_i \quad (45)$$

$$r = L_2 \sin \theta_r \quad (46)$$

$$t = L_2 \cos \theta_r \quad (47)$$

Applying Pythagoras' theorem, we derive:

$$(a_1 + L_1)^2 = (dx + r)^2 + t^2 \quad (48)$$

We eliminate higher order terms of  $dx$  and  $a_1$  because they are infinitesimal. Thus, we can obtain:

$$a_1 = dx \sin \theta_r \quad (49)$$

Based on Fermat's principle of stationary phase[39], phase shifts through the two paths are written as:

$$\text{Blue: } L_2 n_1 k_0 + a_2 n_i k_0 + P_2 n_2 k_0 + \varphi + d\varphi = \text{Red: } P_1 n_1 k_0 + a_1 n_i k_0 + L_1 n_i k_0 + \varphi \quad (50)$$

Because  $dx$  is infinitesimal,  $L_2 = L_1, P_1 = P_2$ :

Finally, we shuffle the order of terms in equations (50), we derived Generalized Snell's Law [23]:

$$\sin(\theta_r) - \sin(\theta_i) = \frac{\lambda_0}{2\pi n_i} \frac{d\phi}{dx} \quad (51)$$

where  $\lambda_0$  is wavelength in vacuum,  $n_i$  is the refractive index of incident medium,  $\frac{d\phi}{dx}$  is the phase gradient interface,  $\theta_r$  is reflection angle and  $\theta_i$  is the incident angle. Theoretically, reflection angle can be steered by mapping phase gradient on the interface, where this phenomenon is called anomalous reflection.

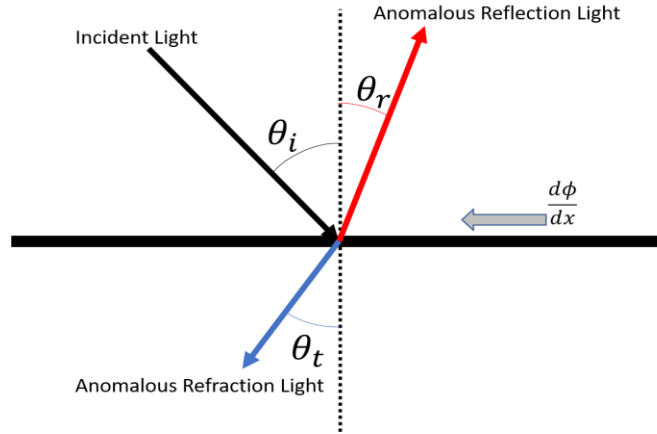


Figure 7: Schematic to Anomalous reflection.

In our meta-form NEV, anomalous reflection and Generalized Snell's Law is the most significant theory to support our design.

## 2.3 EVALUATORS TO NEV

### 2.3.1 Modulation Transfer Function

Modulation Transfer Function (MTF) is a concept born from linear system theory. It is originally used to analyze response from a linear time-invariant (LTI) system. Normally, MTF is valid in a system only when the system satisfies at least four requirements: 1. Detector receives signal directly. 2. Signal is linearly

modulated. 3. Output space is time-invariant. 4. Transfer in system is single-value, i.e. non-noisy. When all these requirements are met, MTF can truly reflect the quality of a system.

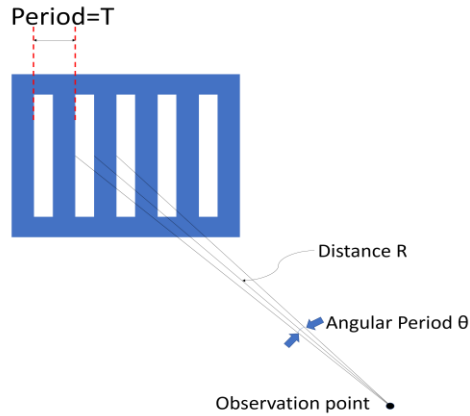


Figure 8: Definition of spatial frequency.

Definition of MTF is the same in an optical system. MTF represents the ability of the optical system to handle spatial frequency. Spatial frequency is defined as number of period among unity spatial distance, shown in figure below.

Spatial frequency  $f_x$  is defined as reciprocal of period T. In practice, unit of spatial frequency is cycles or loops per millimeter. Sometimes, angular frequency is more useful. Angular frequency is defined as:

$$f_{\theta x} = 1/\theta_x = R/T_x \quad (52)$$

Quantitatively, MTF is defined as the ratio of contrast in image space to object space. Here, contrast, also called modulation depth, is determined by the difference of maximum energy to the minimum energy:

$$M = \frac{\max - \min}{\max + \min} = \frac{(b_0 + b_1) - (b_0 - b_2)}{(b_0 + b_1) + (b_0 - b_2)} \quad (53)$$

where  $b_0$  is average energy,  $b_1$  is difference between maximum to average and  $b_2$  is difference between average to minimum.

$$MTF(f_x) = \frac{M_i}{M_0} \quad (54)$$

For example, let us assume that the energy distribution in object space is cosine:  $O(x) = b_0 + b_1 \cos(2\pi f_x x)$  (55). Accordingly, contrast of object space is  $M_O = \frac{b_1}{b_0}$ . Energy distribution in image space can be calculated by convolution of energy distribution (equation 55) and line spread function of the system:

$$I(x) = \int h(\delta) O(x - \delta) d\delta \quad (56)$$

$h(\delta)$  is line spread function. We plug equation (55) into the integral above. After normalization, we have:

$$I(x) = b_0 + b_1 |H(f_x)| \cos[2\pi f_x x - \varphi(f_x)] \quad (57)$$

In equation (55),

$$|H(f_x)| = [H_c^2(f_x) + H_s^2(f_x)]^{1/2} \quad (58)$$

$$H_c(f_x) = \frac{\int h(\delta) \cos(2\pi f_x x) d\delta}{\int h(\delta) d\delta} \quad (59)$$

$$H_s(f_x) = \frac{\int h(\delta) \sin(2\pi f_x x) d\delta}{\int h(\delta) d\delta} \quad (60)$$

$$\cos[\varphi(f_x)] = \frac{H_c(f_x)}{|H_c(f_x)|} \quad (61)$$

$$\tan[\varphi(f_x)] = \frac{H_s(f_x)}{H_c(f_x)} \quad (62)$$

From equations (56) ~ (60), the contrast in image space is written as:

$$M_i = \frac{b_1 |H(f_x)|}{b_0} = M_O |H(f_x)| \quad (63)$$

MTF is obtained by shuffling order of equation (61):

$$MTF(f_x) = \frac{M_i}{M_0} = |H(f_x)| \quad (64)$$

In detail, MTF is one part of the Optical Transfer Function (OTF), where another part is Phase Transfer Function (PhTF):

$$OTF(f_x) = MTF(f_x) \exp[-jPhTF(f_x)] = |H(f_x)| \exp[-j\varphi(f_x)] \quad (65)$$

MTF can be obtained by the Fourier transform of Line (Point) Spread Function of the optical system.

### 2.3.2 Geometric Optics

Wavelength of visible light is much smaller than the size of human's eye, so that geometric optics is applicable. In this chapter, common aberrations in geometric optics are introduced. Among them, distortion is significantly used as one evaluator to a NEV.

Optical aberrations are imperfection of images in an optical system. Here, we only discuss monochromatic aberration, including Distortion, Coma, Spherical Aberration, Astigmatism and Field Curvature.

Firstly, distortion is a special type of aberration, because only distortion does not affect the clarity of image. Distortion makes image dissimilar to the object. Distortion happens due to the difference of magnification on image plane when paraxial approximation is not holding. Some common types of radial distortion are shown in figure below.

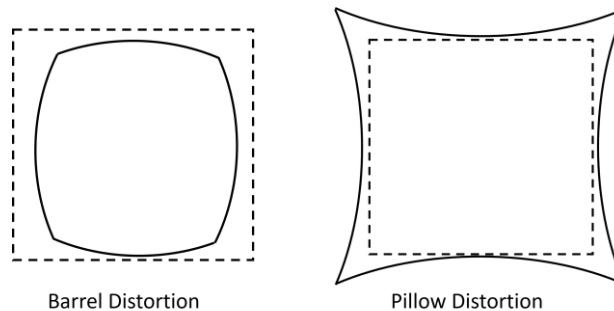


Figure 9: Appearance of two types of common distortion.

Secondly, Field Curvature happens on an object normal to primary optical axis. Rays from this object cannot be perfectly guided onto Gaussian image plane, where Gaussian image plane is a flat surface normal to primary optical axis at the focal point of paraxial rays. We can introduce auxiliary axes in explanation, as shown below.

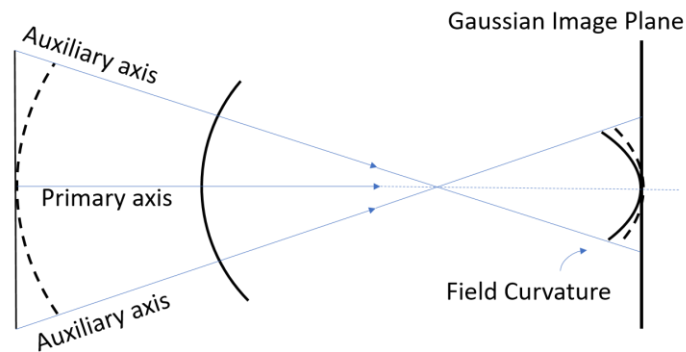


Figure 10: Explanation of how Field Curvature happens.

Thirdly, Spherical Aberration is only related to the size of aperture. Spherical Aberration is formed because of increased refraction at the edge of optical elements. On the edge of large-size optical elements, paraxial approximation does not hold anymore. Hence, rays are deviated from the focal point where lights should focus based on paraxial approximation.

Fourthly, astigmatism is familiar to people because it is common in human's eyeball. Astigmatism is described as the foci on tangential plane and sagittal plane are at different positions on the optical axis. On either horizontal direction or vertical plane, rays can focus separately but not for both at the same point.

Finally, Coma is resulted from off-axis light source and it looks like a comet having a tail. Coma can be described as various magnification on entrance pupil of an optical system, so that rays are not focused on Gaussian image plane, as shown below.

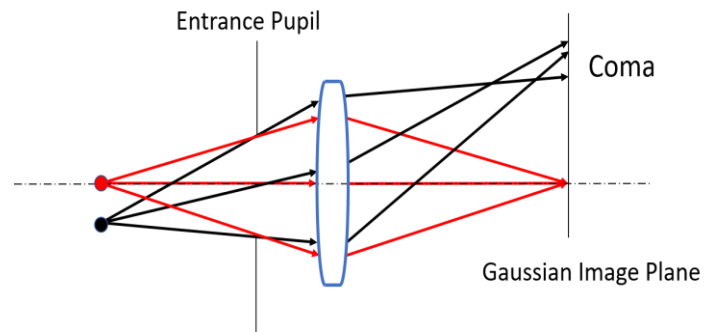


Figure 11: Explanation of how Coma happens.

### 2.3.3 Field of View

Field of view (FOV), sometimes called ‘visual field’, describe the extent of the image space, that can be seen by observers. Human eye has wide monocular or binocular FOV. Monocular FOV is narrower than binocular but higher. Monocular FOV is  $160^\circ$  wide and  $175^\circ$  high and binocular FOV is  $200^\circ$  horizontally and  $135^\circ$  vertically in total [40, 41].

In our design, FOV is the main point to be improved. A limitation on FOV in freeform NEV will be proposed. To overcome this limitation, a meta-form NEV is brought in to replace the freeform NEV.

Quantitatively, FOV is defined as the number of degrees of visual angle during stable fixation of eye [42]. Figure below shows definition of FOV in 3D. In our design, I use horizontal FOV and vertical FOV. However, as for a central symmetric system, such as a circle image space, diagonal FOV is sometimes investigated instead.

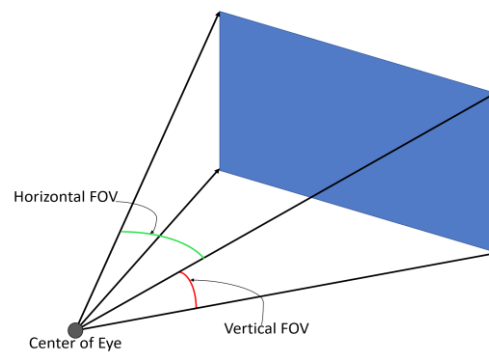


Figure 12: The definition of field of view.

## CHAPTER 3. RESULTS AND SIMULATIONS

Near-eye visor is the central device in a Head-mounted display. Performance of HMD is directly determined by the NEV, because NEV can couple lights from display into human's eye. Besides, the volume of a HMD device is primarily decided by the volume of its NEV, in the same manner as lenses determines the volume of the cameras. Basically, a compact structure of NEV with promising vision performance is desired. Compared with results on multi-element NEV[9, 10, 12-14, 16], we design a single-element NEV to avoid complex structure.

### 3.1 FREEFORM NEV

#### 3.1.1 *Freeform Visor Design and Limitation*

Before introducing metasurface NEV, I design a freeform NEV to verify the methodology to design a NEV. Simultaneously, the limitation on FOV in freeform NEV is proposed.

We first briefly introduce freeform optics. Freeform optical elements are defined as non-rotationally symmetric elements or rotationally symmetric elements with not standard shapes. Phase mask is generally defined as a certain type of freeform optics elements. Complex-shape freeform optics elements are extremely difficult to be fabricated.

In this design, I used Matlab to calculate the FOV and the shape of the freeform visor. Before calculation begins, the size and position for both display and exit pupil are settled. The display is tilted by 45 degrees to shine lights onto visor. Besides, distance from visor to eye is fixed, as well.

In calculation, Matlab code is fed with a value of FOV on horizontal direction and vertical direction. All steps above are shown in figure below:

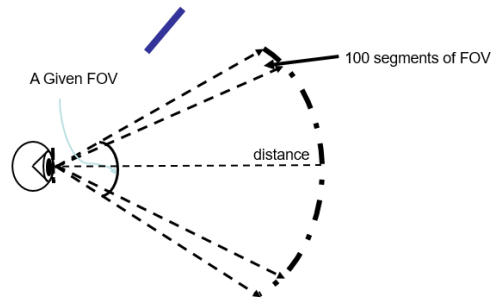


Figure 13: Side view of the schematic of the methodology of designing a near visor.

The keystone to design the NEV is to ensure that light rays pass through the exit pupil parallelly. Hence, we can divide entire FOV on each direction into 1000 segments. At the same time, the display on the same direction is divided into 10 pixels, as well. The numbers of pixels or segments are not fixed. We choose to use 10 and 1000 because they can give smooth visor shape and only take short simulation time.

Next, for one pixel on the display, lights from that pixel will be reflected by a group of 100 segments of visor and propagate through the exit pupil parallelly, as shown in Figure 18 in red lines and purple lines. We can sweep all 10 pixels on the display to form the entire shape of freeform visor, as shown in green curve in Figure 14.

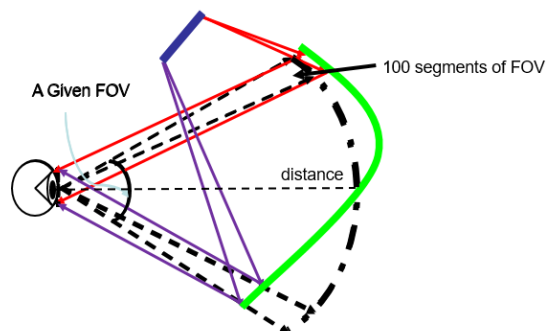


Figure 14: Formation of freeform NEV.

In detail, the size of exit pupil is set as 4mm in diameter. To make a compact structure, distance from eye to visor is set at 30mm. Similar distance was also used in ref.[8]. Display is 15mm away from visor, in between the visor and eye. The display is 15mm decentered from optical axis upward and tilted by  $45^\circ$ . FOV fed into Matlab are  $60^\circ$  vertically and  $50^\circ$  horizontally.

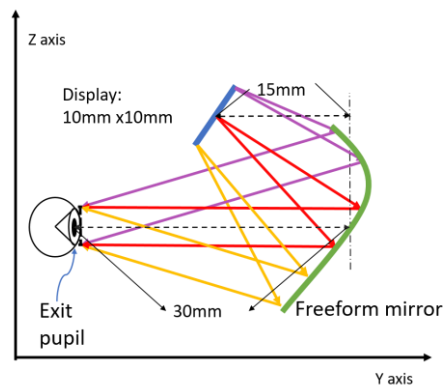


Figure 15: The schematic of freeform NEV.

Shape of freeform NEV is calculated and plotted in Figure 16. The green surface is the freeform visor, blue flat surface is microdisplay and red star is the center of exit pupil.

By using Matlab, we calculated the working FOVs are  $62.59^\circ$  vertically and  $53.02^\circ$  horizontally.

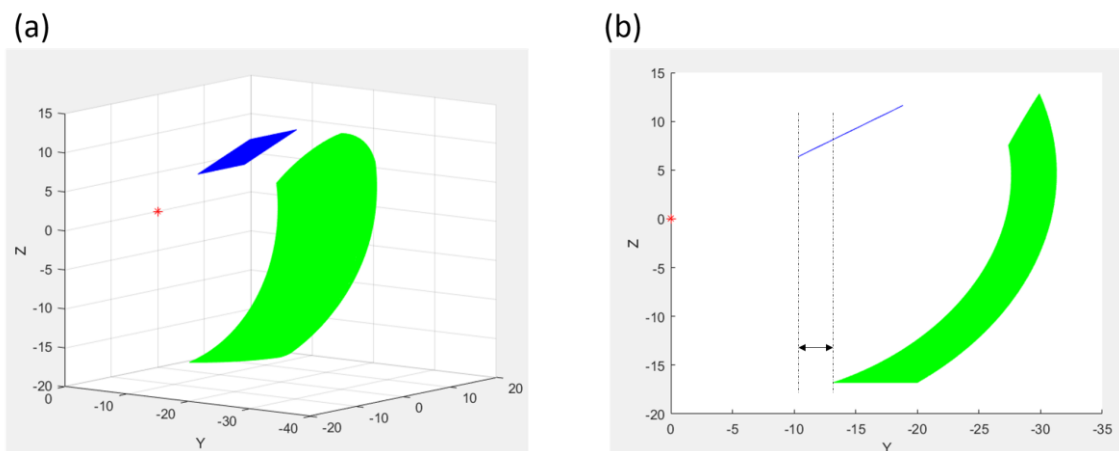


Figure 16: Matlab result of (a)3D and (b) side view of freeform NEV system.

Besides, we can see the highly curved shape of freeform NEV when the freeform visor is designed to give a large FOV. Especially in the Y direction, the edge of visor is almost touching the edge of the display, which are shown by the dotted line in Figure 16(b). If this shape of freeform NEV is with such a high curvature, it is problematic in fabrication, in practice. It will cost a lot, as well[12]. When we want to bring the visor closer to human's eye, curvature of visor will increase and a serious problem emerges.

We find that, as we bring the visor closer, the light ray needs to be bent by larger angle, and often the mathematical solution becomes unphysical, as shown in Figure 16. Hence, we can only get a vertical FOV of  $63^\circ$  and horizontal FOV of  $52^\circ$ . Further increase in the FOV results in an unphysical solution: the shape of the visor extends beyond the edge of display reaching backside

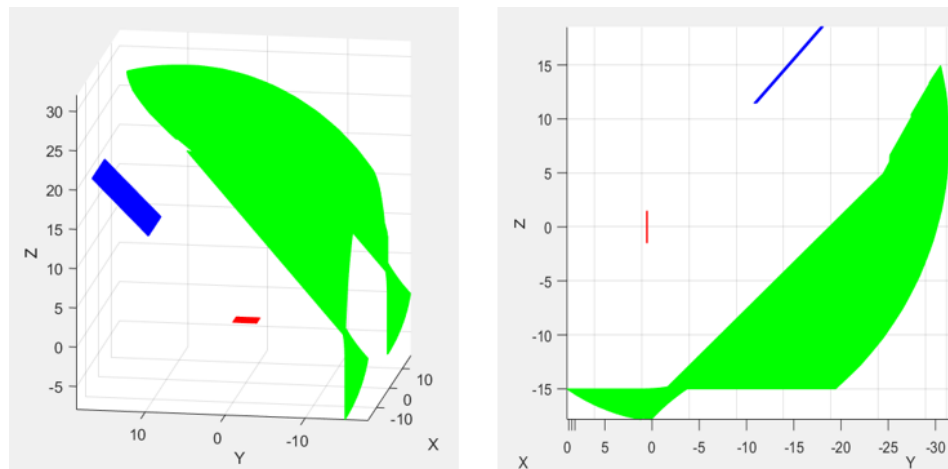


Figure 17: Physically invalid solution for freeform NEV as large FOV given.

of display. This limitation comes from the fact that the light guiding principle is based on reflection, and the light cannot be bent arbitrarily.

So far in summary, a freeform NEV is designed to have  $62.59^\circ$  vertical and  $53.03^\circ$  horizontal FOV. More importantly, we reveal and explain the limitation on FOV for freeform NEV. Because its incapability to steer light in arbitrary direction, we can only modify the shape of visor to change

direction of reflection light, leading to high curvature of visor. After the visor reaches the backside of display, solution for the freeform NEV becomes physically meaningless.

### 3.1.2 Freeform Visor Performance

The freeform visor with 62.59° vertical and 53.03° horizontal FOV is simulated in Zemax. MTF and Grid distortion are extracted from the simulation.

As the shape of visor is not a standard shape or governed by a certain mathematical expression, we use curve fitting to reproduce the freeform visor in Zemax. Using application ‘Curve fitting’

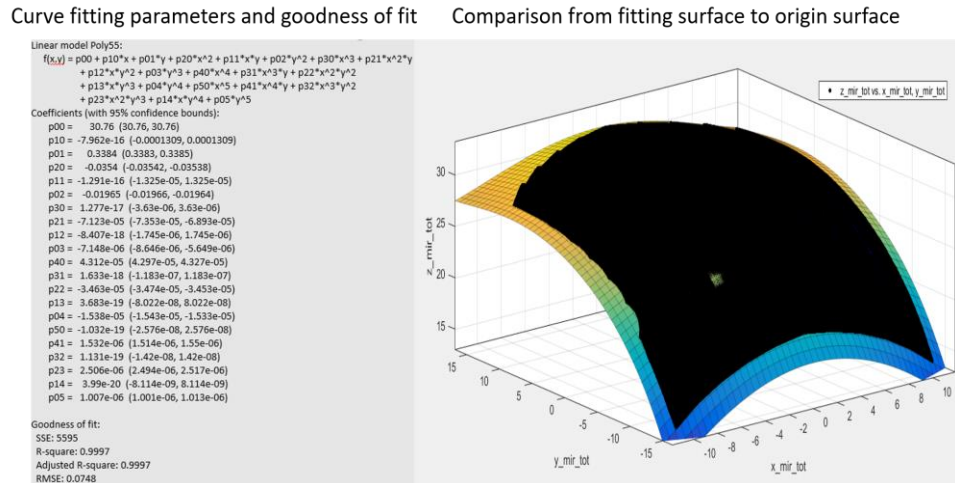


Figure 18: Results from curve fitting, black surface being original and colored surface being fitted.

default in Matlab, a fifth-order polynomial is obtained with high enough accuracy. Goodness of curve fitting is shown in Figure 18.

In Zemax, an ‘Extended Polynomial Surface’ is used to draw the freeform visor.

From Zemax, MTF and distortion are shown in Figure 19. In MTF figure, lines with different color are from different positions where the MTF is measured. 5 positions are shown in the inset with different colors. Dotted line of MTF stands for MTF on tangential plane and solid line stands for sagittal plane.

MTF curves stay higher than 50% at 23 cycles/mm and drop to lower than 10% at around 33 cycles/mm. The Grid Distortion is around 6% maximum at corners. FOV, as shown in the previous chapter, is around  $63^\circ$  vertically and  $53^\circ$  horizontally. Similar result for MTF and distortion can be found from [8], 7.4% maximum Grid Distortion on Magnifier Surface and comparable values

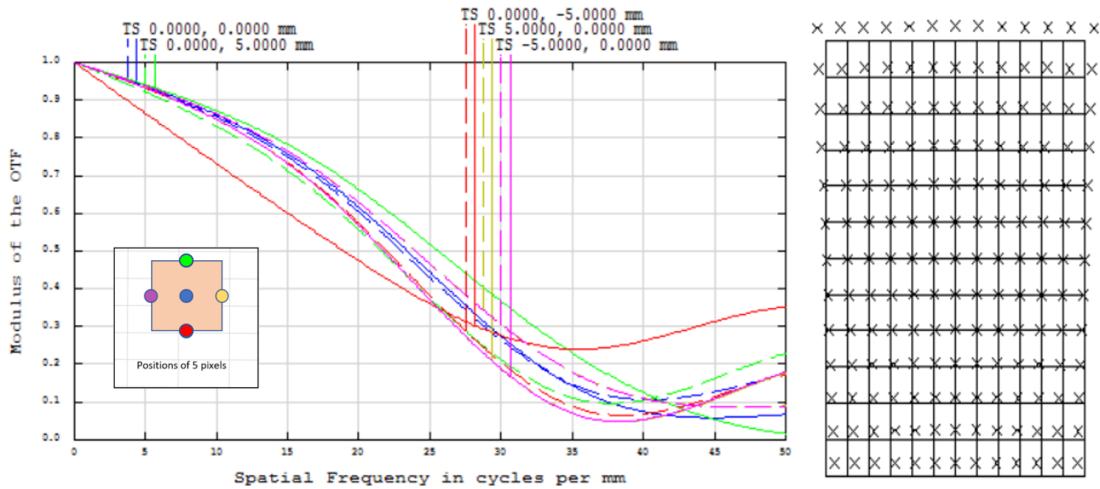


Figure 19: Vision performance of freeform NEV.

of MTF. However, FOV in [8] is  $24^\circ$  diagonal, because they design their NEV in a round shape. Due to their smaller size of visor, with 14mm diameter, and similar distance from eye to visor as around 32.9mm, their smaller FOV is understandable.

However, in practice, it is not only difficult to fabricate a large-size freeform visor for large FOV, but also the FOV itself is limited by the increasing curvature of freeform visor. Besides, if the visor is needed to be brought closer to eye, FOV is limited by high curvature visor intensely.

To overcome this limitation on FOV, the shape of visor is needed to be modified. Here, I propose my solution for NEV. A metasurface reflector is used to replace the freeform visor, because metasurface is a flat and efficient optical system to implement spatial transfer to incident light wave. The flat nature of metasurface is very suitable in NEV for high FOV and ultra-compact system.

## 3.2 META-FORM NEV

### 3.2.1 Meta-form Visor Design

A design of NEV based on metasurface freeform optics is explained here, termed as meta-form optics with a thickness of only a micron [24]. The extreme thinness of the meta-form visor and flat geometry allow them to be integrated with flexible substrate[43, 44]. Thus, one can vision building a sticker-like visor element, which can be placed on any eye-wear to convert them to a NEV.

Based on introduction from Chapter 2, Generalized Snell's Law [23] blazes a brand new trail to design the meta-form visor, using phase mask. Metasurface is a suitable platform to generate the phase mask.

Two choices are available to optimize the FOV of NEV. We can either enlarge the size of meta-form visor at the same distance from eye to visor, or we can close the distance from visor to eye when we keep size of visor unchanged. Here, we chose to do both optimization. We brought visor closer to eye and design a larger size of visor than freeform visor. As shown in Figure 20, distance from visor to eye is shortened to 25mm and size of visor is designed to be 40mm by 40mm. Size and position of display is kept the same.

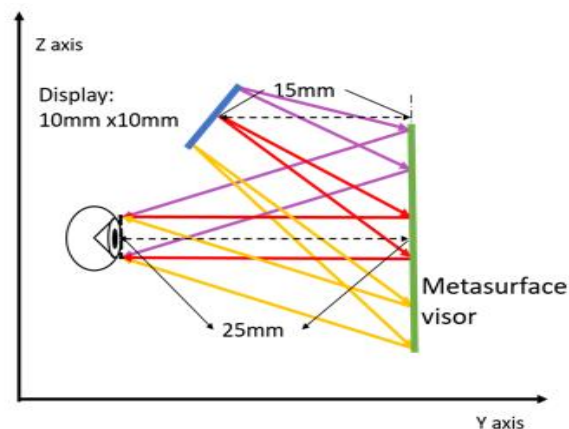


Figure 20: Schematics of meta-form visor on XZ plane.

From Matlab, the FOV is  $77.32^\circ$  both vertically and horizontally.

3D schematic of meta-form NEV from Matlab is shown in Figure 21. The gradual color changing surface is display, green surface is the visor and red square is the exit pupil of this system, as well as the entrance pupil of eye.

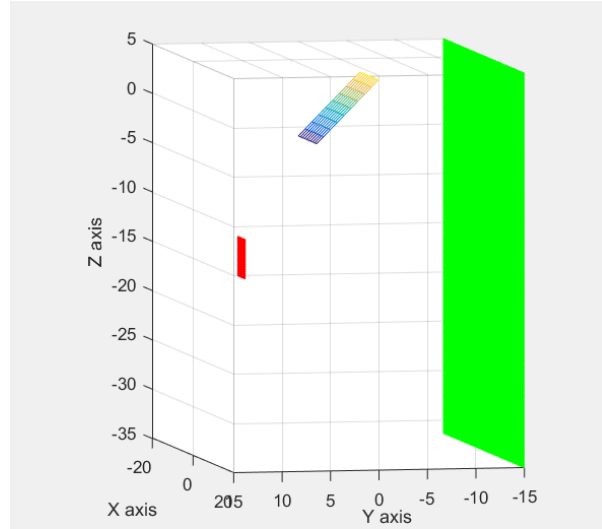


Figure 21: 3D schematic of meta-form NEV.

Until here, in summary, the geometry of visor is successfully settled. Based on the geometry we set, FOV are  $77.32^\circ$  both vertically and horizontally. We brought visor closer to eye and enlarge the size of visor to obtain a large FOV, as well.

### 3.2.2 Phase Distribution on Meta-Form Visor

Based on Generalized Snell's Law [23] and anomalous reflection phenomenon, direction of reflection lights can be steered by phase gradient on interface.

The relationship between reflection angle, incident angle, wavevector and phase gradient is revealed as below, where we choose to use red light at 633nm wavelength and refractive index being 1.

$$\sin(\theta_r) - \sin(\theta_i) = \frac{\lambda_0}{2\pi n_i} \frac{d\phi}{dx} \quad (66)$$

Because we have settled the position and size of every components in the system, reflection angle  $\theta_r$  and incident angle  $\theta_i$  are easy to be calculated. In detail, the algorithm to calculate phase distribution on the phase mask is similar to how we calculate the shape of freeform visor. However, we are mapping out phase distribution through relationship between angles and phase gradient, and not finding spatial coordinates of points on visor. Hence, the first step is to set an initial value of phase, where for simplicity we chose it to be 0. Although initial value will not affect the phase gradient and reflection angle, it influences the absolute value of phase and results after phase wrapping is applied on phase distribution.

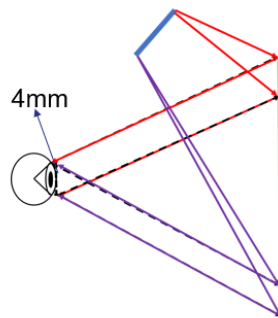


Figure 22: Methodology of phase calculation.

Figure 22 shows the methodology of phase calculation.

In meta-form NEV, lights should go through exit pupil parallelly, as well. We divide the entire length of visor into 1000 segments. The display is also divided into 10 pixels. Based on our geometry, the size of visor is 40mm and exit pupil is 4mm. Hence for every 100 segments on the visor, their size is the same as the size of the exit pupil. Lights from the first pixel on the display are reflected by the first 100 segments of visor, and go through the eye pupil parallelly, as shown in Figure 22 by red light rays. Incident angles and reflection angles are easily calculated and substitute into Generalized Snell's Law, so that phase gradient is calculated. By sweeping the ten pixels on display and all 1000 segments of visor, the entire phase distribution on one direction is

obtained. On the other direction, phase is calculated in the same manner. Finally, we add up phase values on both directions point by point to form the final phase mask.

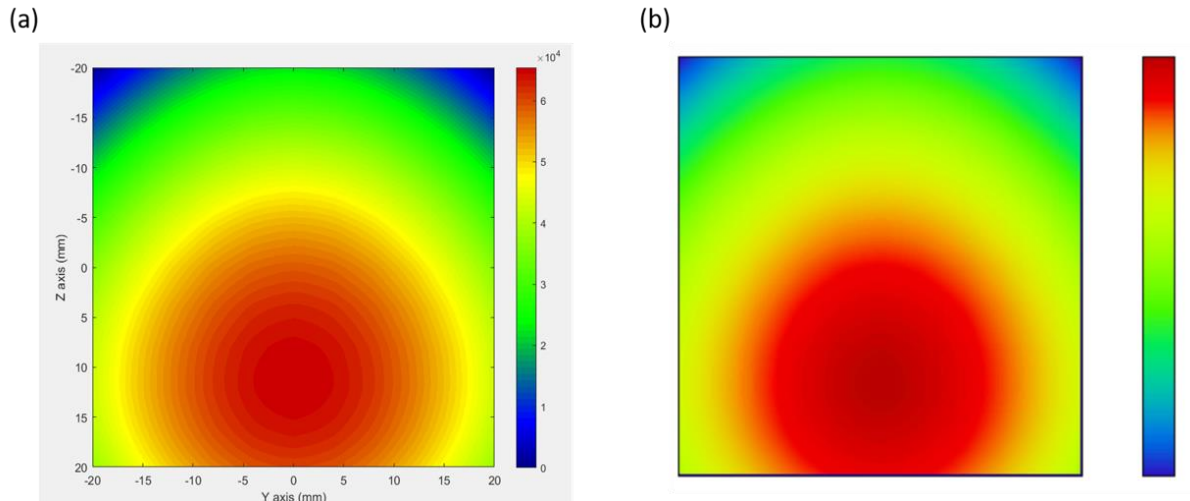


Figure 23: Phase profile.

Phase distribution on meta-form visor is shown in Figure 23. Unit of phase here is not in radian, but in the periods of  $2\pi$ . Magnitude of phase goes to  $6.7 \times 10^4$  times of  $2\pi$ , due to large scale of visor compared with wavelength.

Curve fitting is not used in phase mask, because phase data from Matlab are just imported into Zemax using 'import data'. Phases imported in the Zemax are on the right side.

### 3.2.3 Meta-form Visor Performance

In this chapter, the meta-form NEV is simulated in Zemax. MTF and Grid Distortion are extracted.

Again, different colors on MTF correspond to different positions where the MTF is extracted. MTFs for sagittal plane and tangential plane are shown in different figures for clarity. MTF keeps beyond 50% at 50 cycles/mm and dive under 10% at 80 cycles/mm.

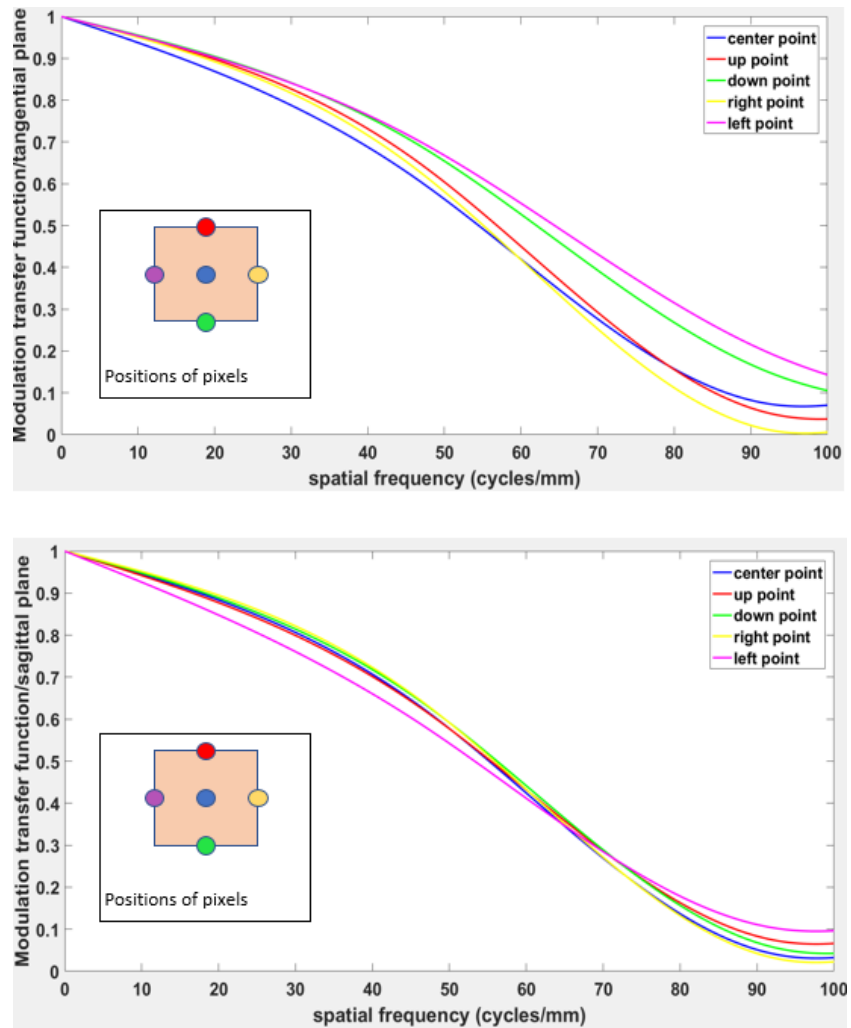


Figure 24: MTF of NEV.

MTF of meta-form NEV is higher than results from freeform NEV, which means meta-form NEV can handle more elegant structures in object space.

Grid Distortion is shown in Figure 24. The largest distortion happens on the corner of image, which is 8.7626%. Unlike MTF, Grid Distortion does not represent clarity of image but just brings in dissimilarity on shape of image compared to objects. Distortion can be recovered by applying pre-processing to images on display to revise the dissimilarity.

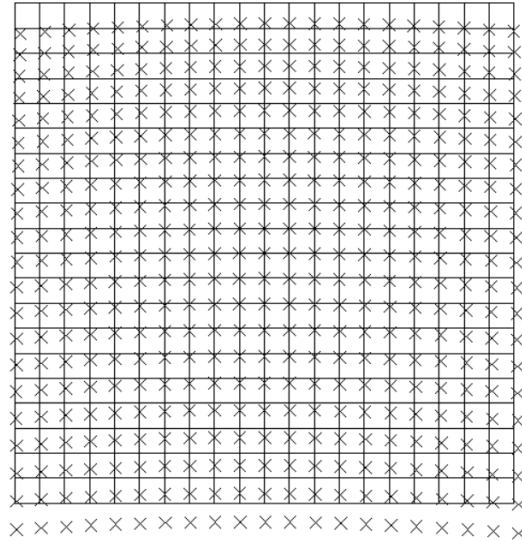


Figure 25: Grid Distortion of NEV.

Same as calculated from Matlab, FOV is  $77^\circ$  both vertically and horizontally, as well.

Besides, ray tracing is also performed in Zemax, and its result is shown in Figure 26. Lights from display are reflected by visor anomalously and go through exit pupil of eye parallelly. Parallel lights are converged by lens in eyeball and focus on retina. On the display, the order of pixel array is colored by purple, golden, red, green and blue from top to bottom. However, on retina, the order is reversed. Thus, the image on retina should be upside down and leftside right compared to image on the display.

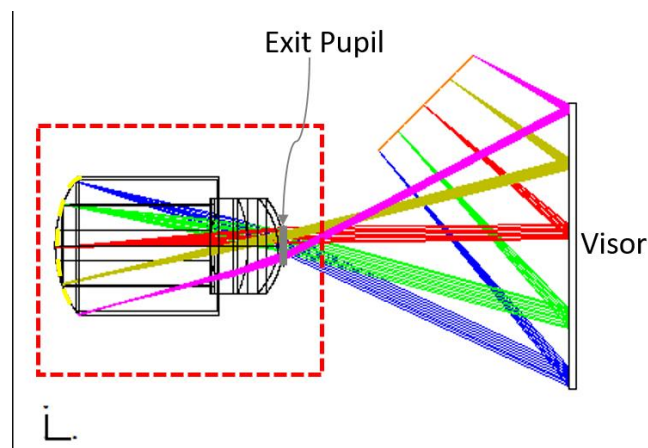


Figure 26: Ray tracing of NEV.

In Figure 26, the eye model is highlighted inside the dotted red square. This eye model is constructed on basis of Liou & Brennan 1997 eye model[45]. In detail, this eye model is drawn in Figure 27. We can see parallel incident light into eyeball are focused well on retina, which indicates the model is trustable

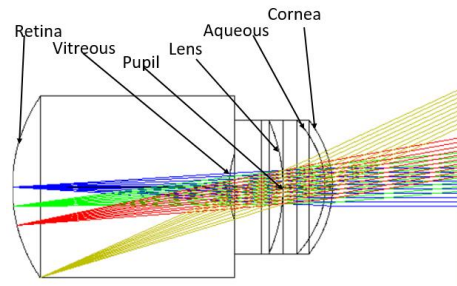


Figure 27: Liou & Brennan 1997 eye model.

Finally, an image of Mona-Lisa is simulated through the meta-form NEV. Simulated image of Mona-Lisa is shown in figure below. The left picture is the original figure I feed into simulation, and right one is the image output. We can see the color of the image is red, because this meta-form visor is designed in red light wavelength. Secondly, this image suffers distortion, especially at corner. From Grid Distortion, we see maximum distortion at corner, as well. However, such distortion can be easily revised by applying pre-processing on original image input. For example, we see the image output suffer ‘image warping’ and it can be recovered by applying a simple ‘de-warping’ on original image. Besides, clarity of image is well maintained, consistent with the previously calculated high-quality MTF.



Figure 28 Image simulation of Mona-Lisa.

### 3.3 METASURFACE DESIGN

So far, the phase mask of my meta-form visor has been created and simulated. Those promising results indicate its potential to be applied in vision system. Here, I choose to use metasurface to realize this phase mask.

Metasurface is a 2-dimensional array of subwavelength scatterers. The top view and side view of a metasurface is shown in Figure 29. For one unit cell of metasurface, it is a squared shape with side of 450nm. In one unit cell, the silicon cylindrical post ( $n \sim 3.5$ ) is placed on a squared shape silica substrate ( $n \sim 1.5$ ) Thickness of substrate is 633nm, which is one wavelength. Height of the post is 200nm. By changing the diameter of post, these pixels can generate various phase response and amplitude response in reflection.

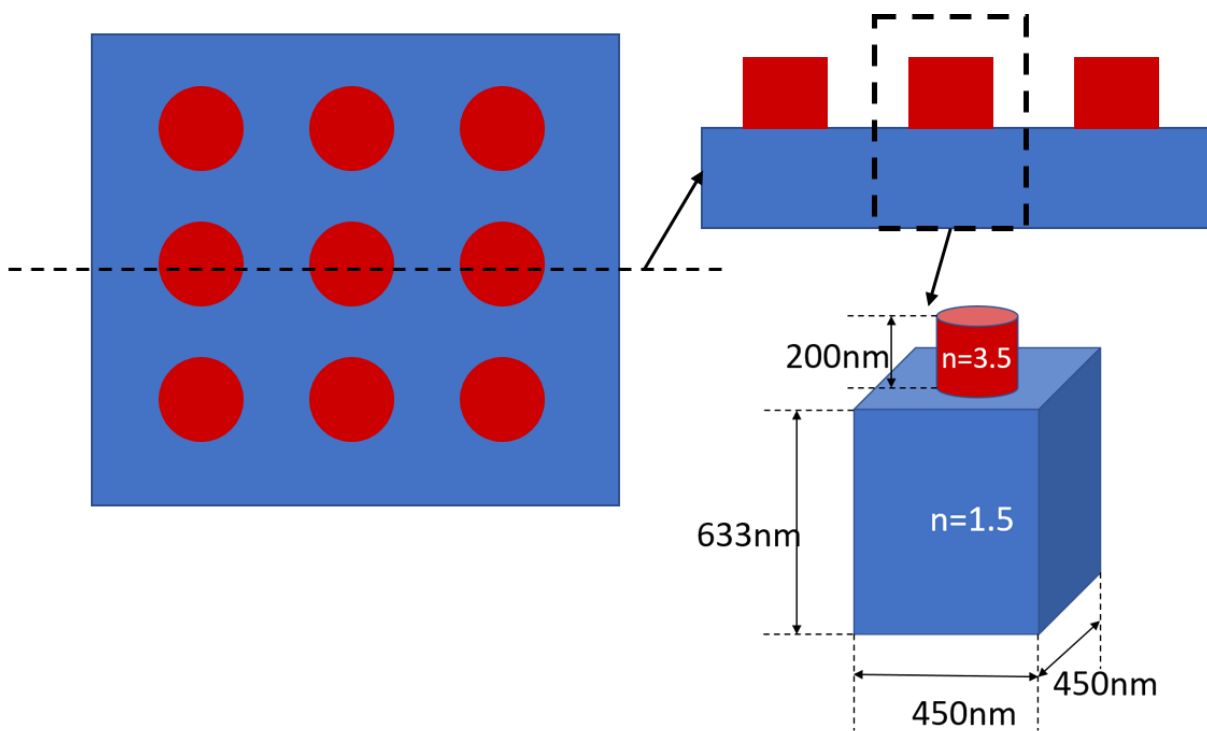


Figure 29: 2-dimensional array structure of a metasurface and one pixel of this type of metasurface.

Rigorous Coupled Wave Analysis (RCWA) simulation is applied to find the relationship between post diameters to phase/amplitude response in reflection. Basically, RCWA is an analytical method in

computational electromagnetic, which is widely used for spatially periodic dielectric structure. The electromagnetic field is decomposed into Fourier's space as the summation of spatial harmonic. Result after RCWA analysis is shown below in Figure 30.

In RCWA result, blue line is the phase response of the reflection light, where unit for phase is period of  $2\pi$ . Green line shows normalized amplitude of reflection light. We can see significant amplitude

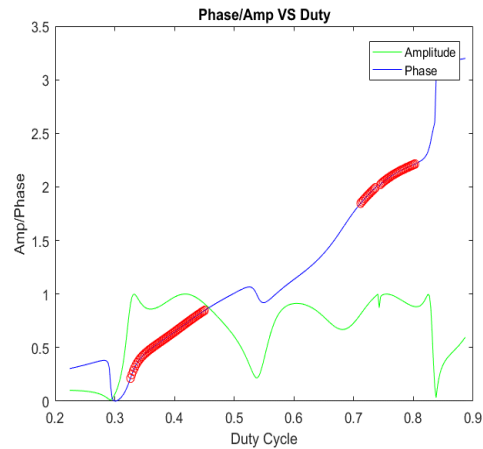


Figure 30: RCWA results, filling factor of one period to phase/ Amplitude response of reflection light.

modulation. This phase value is not applied phase wrapping yet, so it is ranged from 0 to  $6.6\pi$  (3.3 period of  $2\pi$ ). However, phase range from 0 to  $2\pi$  is needed sufficiently for metasurface design. To ensure that our posts can meet both requirements of high enough reflected light intensity and generating phase ranged from 0 to  $2\pi$  simultaneously, we select some sections with both wide enough phase ranges and high amplitude (larger than 0.8) provided. Selected sections are highlighted in red.

Based on the relationship between a specific diameter and phase response, we can map out diameter distribution on the visor after scale-down, as shown in figure below. The entire system is scaled down by 2500 times on each side to save time and memory in simulation. The size of metasurface is 16 microns on each side and there are 36 pixels in total on each side after scale-down.

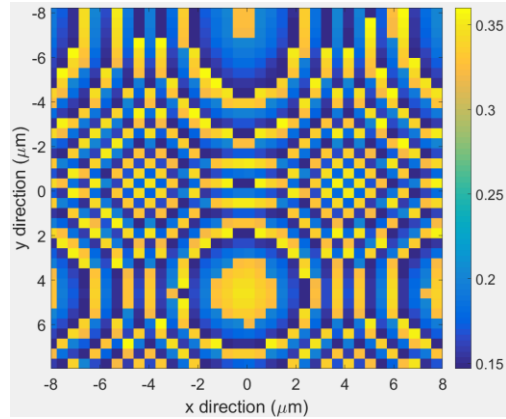


Figure 31: Diameter map of scaled-down metasurface.

### 3.4 METASURFACE NEV IMAGE SIMULATION

Image simulation is performed in Lumerical FDTD software. The scaled-down metasurface works as a visor. The appearance of the metasurface is shown in the figure below. Although the colorbar is denoted by many color, there are only binary types of material in Figure 32. Red dots are those posts with different size, and blue region is air with refractive index equal to 1. The exit pupil of eye is mimicked by a monitor. After having field on exit pupil, we do Angular Spectrum Analysis to calculate field on retina.

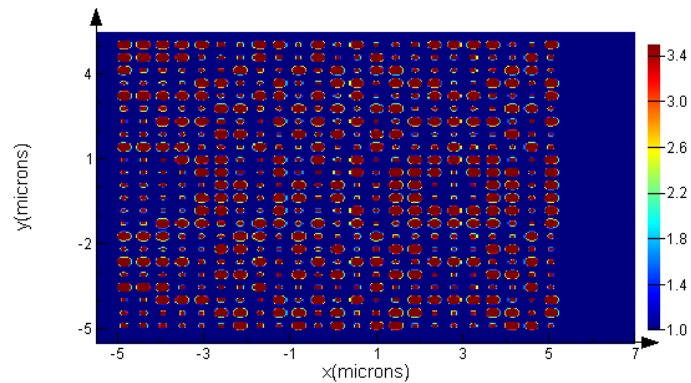


Figure 32: Real appearance of metasurface in Lumerical.

Display is mimicked by a 10 x 10 matrix of Gaussian light sources. When Numerical Aperture of Gaussian beams is properly set, each Gaussian source is clearly separated from other sources, as shown in Figure 33. Here, NA is set to be 0.75 for the clearest image. By changing intensities of certain sources, five different shapes are created for image simulation, which are reverse U, reverse W, round, triangular and rectangular.

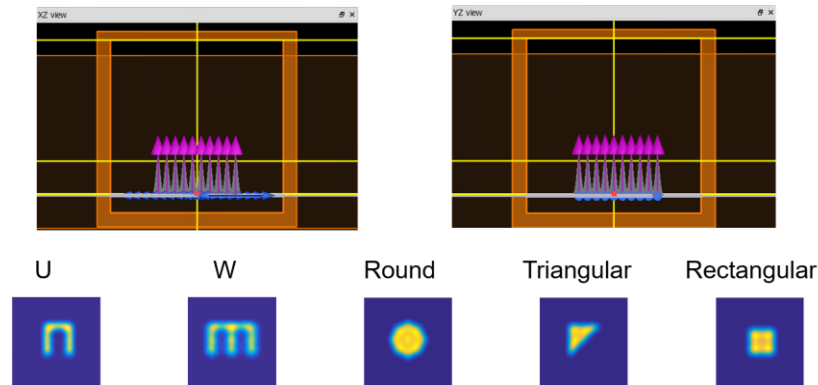


Figure 33: Schematic of display simulation and its result.

In the simulation of NEV system, as mentioned in the previous chapter of meta-form NEV design, the display is tilted by  $45^\circ$  to shine lights onto visor. Position of display is highlighted in yellow in Figure 34.

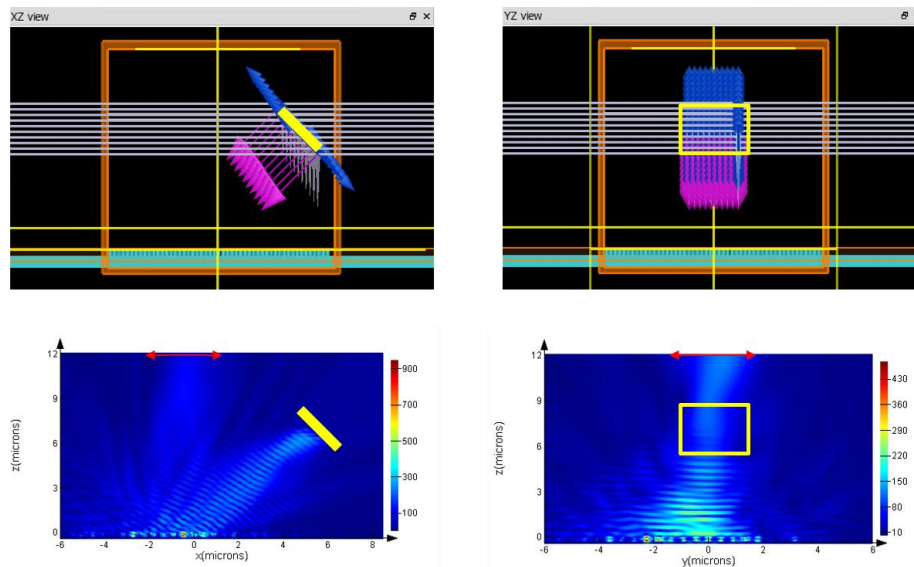


Figure 34: Schematic of the scale-down NEV system and energy distribution from sideview.

From the second row of Figure 34, we can see the energy focus within the region of entrance pupil of eye model, which is marked by red. On the YZ view, although the NEV system is symmetric on Y direction, the energy distribution is not symmetric here, because this sideview is taken from ‘triangular’ shape simulation. The triangular is created asymmetric on Y direction.

We only extract electric field from monitor, because human’s eye only responses to electric field. Angular Spectrum Analysis was applied on extracted data, to mimic light propagating through a lens. In eye model, the human’s eye is always simplified as a lens with 2mm focus length. After scale-down, focal length of eye model becomes  $8\mu\text{m}$ . Basically, Angular Spectrum Analysis expands a complex wave into summation of infinite number of plane waves and transforms them into Fourier Space in function of spatial frequency/ wave vector. Each plane wave is multiplied by propagation terms which are from phase accumulation from original plane to predicted plane. All the results from image simulation are represented below in Figure 35.

In Figure 35, the first row shows the shapes I expect to see in Lumerical on the display. However, because the lack of resolution on this matrix of Gaussian sources, the real image on the display in the simulation are shown in the second row. We can see nonuniformity of intensities, especially on U and W. For example, on the upper edge of the reverse U or W, energy is concentrated at intersections. But energy is low on elsewhere. On the third row, fields on the entrance pupil is shown and area of entrance pupil of eye is marked by the white square. On the last row, images on retina exhibited. Images on retina are all upside-down and leftside-right compared to image on display.

We can see images on retina suffer distortion and reduced clarity. Especially, straight lines became zigzag. We will do discussion on the imperfection.

Firstly, as the entire NEV is scaled down by 2500 times on each side, it becomes 16 micron on each side. Consequently, on each side, there are only 36 metasurface unit cells. Each unit cell does not contain

all phase information over the region it covers, but just expresses the average phase value over its area. Briefly, resolution of metasurface in simulation is not high enough, which is limited by memory of computer. If the NEV is scaled up back to the size as design, we believe this imperfection can be eliminated.

Secondly, resolution of display is not high enough, so that nonuniformity on shapes is influencing quality of images on retina. In practice, resolution of display will be much higher and images are much more uniform. We believe influence from low-resolution display can also be eliminated.

Thirdly, reflection from substrate exists. When lights are normally incident, reflection can be ignored as we designed the thickness of substrate to one wavelength. However, at this  $45^\circ$  incident angle, reflection from substrate exists. But it should not be regarded as the major influence, because intensity from substrate reflection is not high.

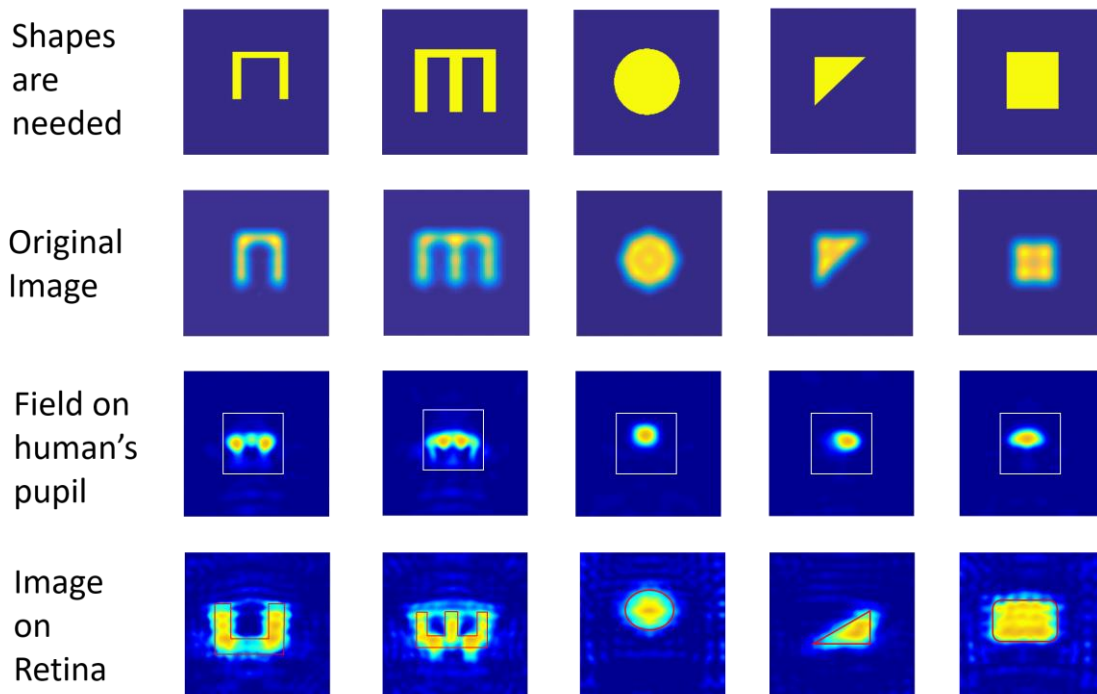


Figure 35: Results of image simulation.

## CHAPTER 4 SUMMARY AND FUTURE WORK

### 4.1 SUMMARY

In this thesis about near eye visor (NEV), a limitation on FOV in freeform NEV is introduced and explained initially. By replacing the freeform NEV with a meta-form NEV, we believe this limitation can be overcome. In our meta-form NEV design, FOV is increased to  $77^\circ$  on both horizontal and vertical directions, which is unable to be reached using freeform NEV at 25 mm distance from eye to visor. Based on Generalized Snell's Law and anomalous reflection, the phase mask for meta-form visor is designed. Ray optics simulation is performed in Zemax using this phase mask. From this simulation, MTF is over 50% at 50 cycles/mm, which is adequate for vision system[16]. Distortion is 8.76% maximum at corners. We see ray tracing works in the same manner as human's eye, as well.

Next, we moved from ray optics to electromagnetism to realize our phase mask. We designed metasurface, which is a suitable platform to realize the phase mask for visor. The metasurface is a array of 200nm high Silicon posts placed on silica substrate. By changing diameter of posts, phase response and reflection amplitude are modulated simultaneously. RCWA numerical simulation was applied to find relationship between various diameters and their phase response.

Consequently, geometries and subwavelength scatterers distribution are obtained. Image simulation is performed in Lumerical FDTD. Metasurface works as visor, a monitor works as entrance pupil of eye and a 10 x 10 matrix of Gaussian sources is mimicking a real display. By applying high intensities on certain sources, five shapes are created and reproduced by visor. Angular Spectrum Analysis is used to mimic light propagating through a lens, where eye model is simplified as a lens. Image on retina is obtained after Angular Spectrum Analysis.

In summary, meta-form visor is capable to overcome the limitation on FOV and to replace freeform NEV, especially in short focal length region. Metasurface, as the optimal platform for meta-form NEV, can enable an ultra-compact structure of NEV to shrink down the volume of NEV or HMD.

## 4.2 OUTLOOK AND FUTURE WORK

There are several improvements which can be applied to this design.

Firstly, in current design, subwavelength post is made of Silicon. However, Silicon provides total reflection for red light, so that the metasurface is totally reflecting. This NEV is suitable for VR technology. For AR technology, it requires a see-through visor to combine the image world and the real world. Hence, Silicon Nitride is another choice to make the metasurface/ visor. There have been research results from our group using Silicon Nitride for metasurface, with low loss in visible light frequency[22]. Although Silicon Nitride is transparent, we can still tune its reflectivity with carefully designing, as shown in the figure below.

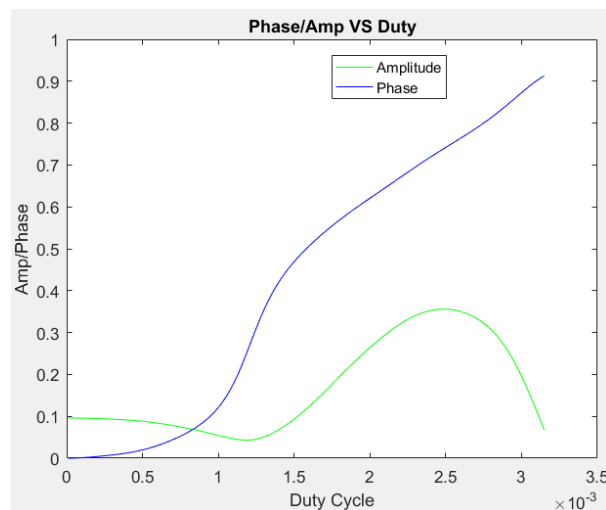


Figure 36: RCWA result of Silicon Nitride post.

Secondly, this Silicon metasurface can be fabricated and tested for VR technology. Recently, VR technology is one of the hottest research topics. The fabrication technology for metasurface is well-developed in our group using single photolithography stage. However, in concern of the size of this meta-form visor, this large-area metasurface fabrication is challenging. The phase mask after phase wrapping is shown below for this large area metasurface.

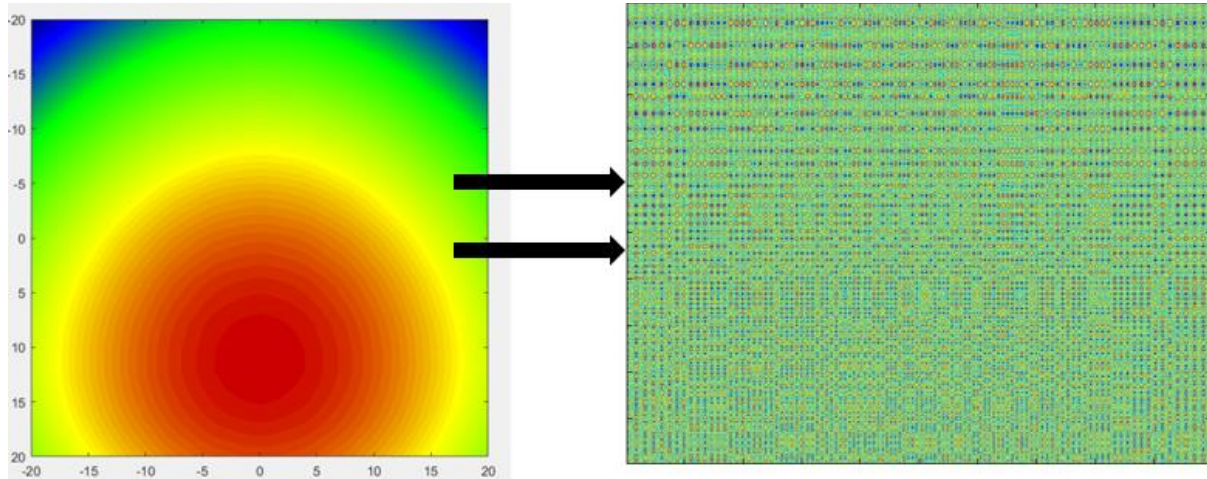


Figure 37: Phase mask after phase wrapping.

Thirdly, in this design, the meta-form visor works under single-wavelength. In practice, an NEV should work at least under RGB wavelengths. Fortunately, there have been results from our group on achromatic metasurface design, which can work for red, green and blue wavelength. Our group has also published results on white light imaging using cubic surface, which is one example of freeform nanophotonics[24].

## BIBLIOGRAPHY

1. *Sony's head-mounted 3D visor is real, HMZ-T1 arrives in Japan November 11th.* 2011, Newstex: New York.
2. Anonymous, *Google "glasses" and privacy.* Policy Options, 2013. **34**(6): p. 63-64.
3. Millman, R., *Microsoft HoloLens: release date, rumours, specs & pricing.* 2015: London.
4. *Sony Corporation*
- Patent Application Titled "Optical Device and Virtual Image Display" Published Online.* 2013: Atlanta. p. 7471.
5. *US Patent Issued to Google on July 19 for "Wearable display device" (California Inventor).* 2016: Washington, D.C.
6. *Microsoft Corporation*
- Patent Application Titled "Wide Field-Of-View Virtual Image Projector" Under Review.* 2013: Atlanta. p. 5868.
7. Saarikko, P., *Diffraction exit-pupil expander with a large field of view.* 2008. p. 700105-700105-6.
8. Cakmakci, O., et al., *Design of a free-form single-element head-worn display.* 2010. p. 761803-761803-6.
9. Cheng, D., et al., *Design of a wide-angle, lightweight head-mounted display using free-form optics tiling.* Optics Letters, 2011. **36**(11): p. 2098.
10. Hu, X. and H. Hua, *High-resolution optical see-through multi-focal-plane head-mounted display using freeform optics.* Optics express, 2014. **22**(11): p. 13896.
11. Pan, J.-W., et al., *Demonstration of a broad band spectral head-mounted display with freeform mirrors.* Optics express, 2014. **22**(11): p. 12785.
12. Yang, J., et al., *Design of a large field-of-view see-through near to eye display with two geometrical waveguides.* Optics letters, 2016. **41**(23): p. 5426.
13. Zhu, Y., et al., *Novel ultra-thin near-eye augmented-view device (UNAD).* Optics express, 2016. **24**(2): p. 1305.
14. Bauer, A. and J.P. Rolland, *Visual space assessment of two all-reflective, freeform, optical see-through head-worn displays.* Optics express, 2014. **22**(11): p. 13155.
15. Bayer, M.M., *Retinal scanning display: a novel HMD approach for Army aviation.* 2002. p. 202-213.
16. Cheng, D., et al., *Design of an ultra-thin near-eye display with geometrical waveguide and freeform optics.* Optics express, 2014. **22**(17): p. 20705.
17. Kenney, M., *The development of metasurfaces for manipulating electromagnetic waves.* 2016, ProQuest Dissertations Publishing.
18. Chen, H.-T., A.J. Taylor, and N. Yu, *A review of metasurfaces: physics and applications.* 2016. p. 076401.
19. Smith, D.R., et al., *Composite Medium with Simultaneously Negative Permeability and Permittivity.* Physical Review Letters, 2000. **84**(18).
20. Fang, N., et al., *Sub-diffraction-limited optical imaging with a silver superlens.* Science (New York, N.Y.), 2005. **308**(5721): p. 534.
21. Schurig, D., et al., *Metamaterial electromagnetic cloak at microwave frequencies.* Science (New York, N.Y.), 2006. **314**(5801): p. 977.
22. Zhan, A., et al., *Low-Contrast Dielectric Metasurface Optics.* ACS Photonics, 2016. **3**(2): p. 209-214.
23. Yu, N., et al., *Light propagation with phase discontinuities: generalized laws of reflection and refraction.* Science (New York, N.Y.), 2011. **334**(6054): p. 333.

24. Zhan, A., et al., *Metasurface Freeform Nanophotonics*. 2016.
25. Heavens, O.S. and S.F. Singer, *Optical Properties of Thin Solid Films*. *Physics Today*, 1956. **9**(3): p. 24-26.
26. Yang, Y., *Resonant All-Dielectric Optical Metamaterials*. 2015, ProQuest Dissertations Publishing.
27. Zhao, Q., et al., *Mie resonance-based dielectric metamaterials*. *Materials Today*, 2009. **12**(12): p. 60-69.
28. Lewin, L., *The electrical constants of a material loaded with spherical particles*. *Journal of the Institution of Electrical Engineers - Part I: General*, 1947. **94**(76): p. 186-186.
29. Slovick, B.A., Z.G. Yu, and S. Krishnamurthy, *Generalized effective-medium theory for metamaterials*. *Physical Review B*, 2014. **89**(15).
30. Stellinga, D., *Shaping light beams with dielectric metasurfaces*. 2016, ProQuest Dissertations Publishing.
31. Menzel, C., C. Rockstuhl, and F. Lederer, *Advanced Jones calculus for the classification of periodic metamaterials*. *Physical Review. A*, 2010. **82**(5).
32. Pancharatnam, S., *Generalized theory of interference, and its applications*. *Proceedings of the Indian Academy of Sciences - Section A*, 1956. **44**(5): p. 247-262.
33. Kildishev, A.V., A. Boltasseva, and V.M. Shalaev, *Planar Photonics with Metasurfaces*. *Science*, 2013. **339**(6125).
34. Colburn, S., A. Zhan, and A. Majumdar, *Tunable metasurfaces via subwavelength phase shifters with uniform amplitude*. 2016.
35. Yang, Y., et al., *Dielectric Meta-Reflectarray for Broadband Linear Polarization Conversion and Optical Vortex Generation*. *Nano Letters*, 2014. **14**(3).
36. Yahyaoui, A., et al., *Numerical analysis of a metasurface based on elliptic dielectric resonators for transmission control of electromagnetic waves*. 2017. p. <xocs:firstpage xmlns:xocs="" />.
37. Armitage, N.P., *Constraints on Jones transmission matrices from time-reversal invariance and discrete spatial symmetries*. *Physical Review B - Condensed Matter and Materials Physics*, 2014. **90**(3).
38. Kang, M., et al., *Wave front engineering from an array of thin aperture antennas*. *Optics Express*, 2012. **20**(14): p. 15882-15890.
39. Tan, A., *Fermat's principle*. *Physics Education*, 1985. **20**(3): p. 103-103.
40. Spring, K.H. and W.S. Stiles, *APPARENT SHAPE AND SIZE OF THE PUPIL VIEWED OBLIQUELY*. *British Journal of Ophthalmology*, 1948. **32**(6): p. 347.
41. Horsager, A. and I. Fine, *The perceptual effects of chronic retinal stimulation*. 2011. 271-300.
42. Adelman, G., *Encyclopedia of neuroscience*, ed. G. Adelman. 1987, Boston: Boston : Birkhäeuser.
43. Ee, H.-S. and R. Agarwal, *Tunable Metasurface and Flat Optical Zoom Lens on a Stretchable Substrate*. *Nano letters*, 2016. **16**(4): p. 2818.
44. Kamali, S.M., et al., *Highly tunable elastic dielectric metasurface lenses (Laser Photonics Rev. 10(6)/2016*. *Laser & Photonics Reviews*, 2016. **10**(6): p. 1062-1062.
45. Smith, G. and D.A. Atchison, *Optics of the human eye*, ed. G. Smith. 2000, Oxford

Boston: Oxford

Boston : Butterworth-Heinemann.